October 1995 • NREL/TP-451-20019

# Photocharge Transport and Recombination Measurements in Amorphous Silicon Films and Solar Cells by Photoconductive Frequency Mixing

## Annual Subcontract Report
## 13 May 1994 - 12 May 1995

R. Braunstein, Y. Tang, S. Dong
*University of California*
*Los Angeles, California*

National Renewable Energy Laboratory
1617 Cole Boulevard
Golden, Colorado 80401-3393
A national laboratory of
the U.S. Department of Energy
Managed by Midwest Research Institute
for the U.S. Department of Energy
under contract No. DE-AC36-83CH10093

NREL/TP-451-20019 • UC Category: 1262 • DE95013131

# Photocharge Transport and Recombination Measurements in Amorphous Silicon Films and Solar Cells by Photoconductive Frequency Mixing

## Annual Subcontract Report 13 May 1994 – 12 May 1995

R. Braunstein, Y. Tang, S. Dong
*University of California*
*Los Angeles, California*

NREL technical monitor: B. von Roedern

National Renewable Energy Laboratory
1617 Cole Boulevard
Golden, Colorado 80401-3393
A national laboratory of the U.S. Department of Energy
Managed by Midwest Research Institute
for the U.S. Department of Energy
under contract No. DE-AC36-83CH10093

Prepared under Subcontract No. XAN-4-13318-10

October 1995

This publication was reproduced from the best available camera-ready copy
submitted by the subcontractor and received no editorial review at NREL.

## NOTICE

This report was prepared as an account of work sponsored by an agency of the United States government. Neither the United States government nor any agency thereof, nor any of their employees, makes any warranty, express or implied, or assumes any legal liability or responsibility for the accuracy, completeness, or usefulness of any information, apparatus, product, or process disclosed, or represents that its use would not infringe privately owned rights. Reference herein to any specific commercial product, process, or service by trade name, trademark, manufacturer, or otherwise does not necessarily constitute or imply its endorsement, recommendation, or favoring by the United States government or any agency thereof. The views and opinions of authors expressed herein do not necessarily state or reflect those of the United States government or any agency thereof.

Available to DOE and DOE contractors from:
Office of Scientific and Technical Information (OSTI)
P.O. Box 62
Oak Ridge, TN 37831
Prices available by calling (615) 576-8401

Available to the public from:
National Technical Information Service (NTIS)
U.S. Department of Commerce
5285 Port Royal Road
Springfield, VA 22161
(703) 487-4650

Printed on paper containing at least 50% wastepaper, including 10% postconsumer waste

# Preface

The prime candidate material for thin-film photovoltaic high efficient solar cells for large-scale power generation is hydrogenated amorphous silicon and alloys. The objectives of the technology in this field are to achieve stable and efficient units for cost effective bulk-power generation. The strategy in this field is to optimize amorphous thin-film growth for greater efficiency and the reduction of light-induced instability. Material preparation efforts of amorphous semiconductors have concentrated on the reduction of "Urbach" edges, sub-bandgap absorption, and the density of deep defects to the end to maximize the photoconductive gain of the material. Most material efforts have been to optimize mobility-lifetime product ($\mu\tau$) as measured by steady state photoconductivity which does not determine $\mu$ and $\tau$ separately. To evaluate various photocharge transport models, it is essential that a simultaneous determination of the mobility and lifetime be performed so as to predict the performance of solar cells. We have developed a photomixing technique to separately determine the mobility and lifetime to characterize materials to predict solar cell performance and to allow the testing of new materials and devices in actual solar cell configurations. The present program forms part of the NREL High-Bandgap Alloy Team and the Metastability and the Mid-bandgap Alloy Team. Various groups are concerned with material synthesis and device fabrication. The UCLA Group performs photoconductive frequency mixing measurements on these material and solar cell devices to determine the optimum growth conditions for photocharge transport. The continuous feedback of the results of the UCLA Group aids synthesis and relates material properties to device performance and gain insight into the light-induced degradation mechanisms.

# Table of Contents

**Page**

**Preface** .......... i

**Table of Contents** .......... ii

**List of Figures** .......... iii

**List of Tables** .......... vi

**Summary** .......... 1

**Introduction** .......... 2

**Photomixing technique for separate determination of mobility and lifetime** .......... 3

Experimental setup of photomixing .......... 11

**Result and analysis** .......... 14

Continuous decay of drift mobility in intrinsic a-Si:H and a-SiC:H upon light soaking investigated by the photomixing technique .......... 14

Effects of deposition conditions on transport properties of intrinsic a-Si:H and a-SiC:H films investigated by the photomixing technique .......... 20

Mobility and lifetime in annealed and light soaked conditions for glow discharge and hot wire intrinsic a-Si:H by photomixing .......... 31

Electric field dependence measurements of mobility .......... 32

Electric fieldd dependence of mobility of compensated a-Si:H samples .......... 40

Light intensity dependence measurements .......... 43

Photoelectron emmission in air from amorphous semiconductors and transparent conducting oxides .......... 48

**Abstract** .......... 60

**References** .......... 61

# List of Figures

Page

Fig. 1 Photomixing signals obtained with a commercial EG&G FND100 diode. The incident laserpower was about 20 mW and the dc bias was 90 V (back biased). The frequencies of the photomixing signals are: 84 MHz, 168 MHz, 252MHz, ... 1.092 GHz. The 252 MHz was the one mostly used, since it has highest intensity. 1 dbm = 1 mW. .......... 4

Fig. 2 Schematic diagram of the photo-generation (1), recombination (2), trapping (3) and thermal emission (4) processes. Only mono-molecular recombination is considered, since it is usually the recombination process with highest probability. $E_{dn}$ and $E_{dp}$ are demarcation energies for electrons and holes. .......... 7

Fig. 3 Block diagram of the experimental setup for photomixing. .......... 12

Fig. 4 The optical setup for photomixing and light soaking. .......... 13

Fig. 5 The dc photoconductivity $\sigma_{dc}$ (a), power of the photomixing signal $P_{mix}$ (b), lifetime $\tau$ (c) and drift mobility $\mu_d$ (d) for the intrinsic a-Si:H sample versus light soaking time. In addition to the decay of the dc photoconductivity and lifetime, continuous decay of the drift mobility can be seen due to light soaking. Solid lines are curve fit to the stretched exponential law (Eq. (22)). Different stretched exponential parameters were found, which are shown in Table 1. The drift mobility $\mu_d$ was determined by Eq. (17) and $\sqrt{\langle\sigma_{ac}^2\rangle}$ was determined by $P_{mix}$. .......... 15-18

Fig. 6 The dc photoconductivity $\sigma_{dc}$ (a), lifetime $\tau$ (b), and drift mobility $\mu_d$ (c) for the a-SiC:H sample versus light soaking time. In addition to the decay of the dc photoconductivity and lifetime, decay of the drift mobility can be seen due to light soaking. Solid lines are curve fit to the stretched exponential law (Eq. (22)). Different stretched exponential parameters were found, which are shown in Table 2. The increase for the drift mobility at $t \sim 100$ min during light soaking is probably due to an increase of the sample temperature upon light illumination and the open circles for the drift mobility were obtained from the dc photoconductivity and curve-fitted lifetime data. .......... 21-23

Fig. 7 Lifetime (at 480 K) of a-Si:H films as a function of deposition temperature. .......... 25

Fig. 8 Drift Mobility (at 480 K) of a-Si:H films as a function of deposition temperature. .......... 26

Fig. 9 Urbach energy of a-Si:H films as a function of deposition temperature. .......... 27

Fig. 10 Lifetime (at 480 K) of a-SiC:H films as a function of hydrogen dilution ratio. .......... 28

Fig. 11 Drift mobility (at 480 K) of a-SiC:H films as a function of hydrogen dilution ratio. .......... 29

Fig. 12 Urbach energy of a-SiC:H films as a function of hydrogen dilution ratio. .......... 30

Fig. 13 Drift mobility versus light soaking time for the hot wire samples at 4 sun light intensit .............. 33

Fig. 14 Drift mobility versus light soaking time for the glow discharge samples at 4 sun light intensity .............................................................................................................. 34

Fig. 15 Drift mobility versus applied electric field for the hot wire samples THD15 (1% H) (a) and THD16 (11% H) (b). Open and solid dots represent the data in the annealed and light soaked state respectively. Solid lines are curve fitting according to Eq. (25) ................................................... 35

Fig. 16 Drift mobility versus applied electric field for the glow discharge samples S#127i (a) and B#1) (b). Open and solid dots represent the data in the annealed and light soaked state respectively. Solid lines are curve fitting according to Eq. (25) ........................................................................ 36

Fig. 17 Electric field dependence of of drift mobility ($\Delta\mu_d/\Delta E/\mu_d$) versusstability (is characterized by the average change in the normalized drift mobility to the change in the electric field, i.e., Dmd/DE/ md, while the stability $(\mu\tau)_{LS}/(\mu\tau)_{AN}$) Of the a-Si:H films under light soaking .............................. 38

Fig. 18 Drift mobility of compensated a-Si:H film with compensation level of $10^{-4}$ versus electric field ................................................................................................................................ 41

Fig. 19 Drift mobility of compensated a-Si:H film with compensation level of $10^{-3}$ versus electric field. ............................................................................................................................... 42

Fig. 20 Drift mobility versus light intensity for the glow discharge sample BK#1. Open and solid circles represent the annealed and light soaked (4 sun, 4 hours) state respectively ............................ 44

Fig. 21 Drift mobility versus light intensity for the hot wire sample THD16. Open and solid circles represent the annealed and light soaked (4 sun, 7 hours) state respectively ............................ 45

Fig. 22 Drift mobility versus light intensity for the hot wire sample THD15. Open and solid circles represent the annealed and light soaked (4 sun, 7 hours) sate respectively ............................. 46

Fig. 23 Drift mobility versus light intensity for the Solarex samples. Open and solid circles represent sample D1203-2 and sample D1203-3 respectively in the light soaked (1 sun, 600 hours) state ............................................................................................................................... 47

Fig. 24 nhomogeneity of NREL a-Si:H film detected by the Optical Stimulated Electron Emission (OSEE) technique ......................................................................................................... 49

Fig. 25 Photoemission in air from sample 4376-21: 200 Å of a-SiC p-layer deposited at IEC on layer 4375-22, texture ZnO from Harvard (Prof.Gordon's Group) ........................................................ 52

Fig. 26 Photoemission in air from sample 4376-11: 200 Å of a-SiC p-layer deposited at IEC on sample 4375-11, textured $SnO_2$ from Solarex (standard device substrate) ............................................. 53

Fig. 27 Photoemission in air from sample 4376-12: 200 Å a-SiC p-layer deposited at IEC on layer 4375-12, textured ZnO from Solarex ......................................................................................... 54

Fig. 28 Photoemission in air from sample 4376-22: 200 Å a-SiC p-layer deposited at IEC on 4375-22, textured layer ZnO from Harvard (Prof. Gordon's Group) ..... 55

Fig. 29 Comparison of the photoemission in air between samples:
4375-11: textured $SnO_2$ from Solarex (standard device substrate) and
A: virgin sample of 4375-11 ..... 56

Fig. 30 Comparison of the photoemission in air between samples:
4375-12: textured ZnO from Solarex,
4375-22: textured ZnO from Harvard (Prof. Gordon's Group), and
B: virgin sample of 4375-21 ..... 57

Fig. 31 Comparison of the photoemission in air between samples of:
91539-21: 1000 Å, specular ZnO (no texture) sputtered at IEC,
91552-17: 200 Å, specular ZnO sputtered on textured $SnO_2$,
91554-04: 1000 Å, specular ZnO sputtered on textured $SnO_2$ and
E: 1000 Å, specular $SnO_2$ grown on textured ZnO (Harvard) ..... 58

Fig. 32 Comparison of the photoemission in air between samples:
A: virgin sample of 4375-11,
C: virgin sample of 4375-21,
4375-11: textured $SnO_2$ from Solarex (standard device sample), and
4375-21: textured ZnO from Utility PV group (UPG) ..... 59

# List of Tables

Page

Table 1 Summary of results from the curve fit for a-Si:H. ..... 12

Table 2 Summary of results from the curve fit for a-SiC:H. ..... 12

Table 3 Sample characterization ..... 31

Table 4 Experimental and curve fitting results for electric field dependence of mobility ..... 39

# Summary

The continuous decay of electron drift mobility in intrinsic a-Si:H and a-SiC:H upon light soaking was investigated by the photomixing technique. The photoconductivity, lifetime and drift mobility in intrinsic hydrogenated amorphous silicon (a-Si:H) and hydrogenated amorphous silicon carbide (a-SiC:H) while light-soaking were determined using a photomixing technique. In addition to the decay of the photoconductivity and electron lifetime, continuous decay of the electron drift mobility was found during the light soaking process, which reveals a new phenomenon associated with the Staebler-Wronski effect. The drift mobility decreased by a factor of 2 for 20 hour light soaking at 2.5 sun intensity. Experimental data were fitted to a stretched exponential law. Different stretched-exponential parameters for photoconductivity, lifetime and drift mobility were obtained, which indicates the production of defects with different generation kinetics upon light soaking.

The effects of deposition conditions on transport properties of intrinsic a-Si:H and a-SiC:H films were investigated by the photomixing technique. By using the photomixing technique, we have determined the electron drift mobility, lifetime and the conduction band Urbach energy (~ 0.1 eV below the band edge) of a-Si:H and a-SiC:H films as a function of deposition temperature ($T_s$, $200C \leq T_s \leq 280C$) and hydrogen dilution ratio (R, $0 \leq R \leq 25$), respectively. We have found that for the a-Si:H films with increasing deposition temperature, the lifetime (at 480 K) increases, both the drift mobility (at 480 K) and the Urbach energy decrease; and for the a-SiC:H films with increasing hydrogen dilution ratio, both the drift mobility (at 480 K) and the lifetime (at 480 K) increase, and the Urbach energy shows a tendency to decrease. These results, together with previous results of other workers, indicate that for the a-Si:H films with increasing deposition temperature, the density of negatively charged defects increases and the density of positively charged and neutral defects decreases; and for the a-SiC:H films with increasing hydrogen dilution ratio, the density of positively charged, negatively charged, and neutral defects all shows a tendency to decrease.

By using the photomixing technique we have found that the drift mobility ($\mu_d$) of intrinsic hydrogenated amorphous silicon (a-Si:H) films produced by both glow discharge and hot wire techniques increases with increasing electric field, while the lifetime ($\tau$) decreases with increasing electric field, and the $\mu\tau$ product is essentially independent of the electric field. We have also found that a greater field dependence of the drift mobility of an a-Si:H film in the annealed state indicates a poorer stability of the photoconductivity upon light soaking. This empirical relationship is consistent with earlier observation that light soaking decreases of the drift mobility in most a-Si:H based materials. This empirical relationship suggests that the Staebler-Wronski degradation of a-Si:H can be linked to defects that are responsible for the field dependence of the drift mobility in the annealed state. Important applications of this empirical relationship include the possibility of assessing the amount of expected light induced degradation without going through time consuming light soaking experiments and possible *in situ* evaluation of stability, e.g., during sample preparation processes to find the optimal conditions for stable samples.

In-air scanning photoemission measurements of bare and a-Si:H coated transparent conductive oxide surfaces revealed inhomogeneities of composition or surface contaminates.

# Introduction

The research pursued during Phase I were part of a collaboration with members of the NREL Wide-bandgap Alloy Team and the Metastability and Mid-bandgap Alloy Team. The tasks were concerned with the characterization of the photoconductivity as a function of temperature of a-Si:H and a-SiC:H layers so as to deconvolute the mobility-lifetime products into mobility and response time. In addition the changes of the above parameters in detail as a function of light induced degradation were investigated. The continuous decay of the electron drift mobility in intrinsic a-Si:H and a-SiC:H upon light soaking was investigated by the technique of photomixing. In addition the effect of deposition temperature and hydrogen dilution on the transport properties of intrinsic a-Si:H and a-SiC:H was also investigated. The dominant approach to accomplish the tasks of the present phase of the program is the technique of photoconductive frequency to separately determine the drift mobility and recombination time. In the following sections the theory of the photoconductive frequency mixing (photomixing), the experimental configuration and the results of the light degradation studies and the characterization of the photocurrent properties of a-Si:H and a-SiC:H prepared by various growth techniques are presented.

This report describes work performed during the phase I of the program in a number of areas. The technique of photoconductive frequency mixing was employed to separately determine the mobility and lifetime in a-Si:H and a-SiC:H. Light degradation studies reveal in addition to the decay of the photoconductivity and electron lifetime, continuous decay of the electron drift mobility was found during the light soaking process, which reveals a new phenomenon associated with the Staebler-Wronski effect. In addition to the generation of defects as recombination centers, defects as charged scattering centers can also be generated upon light soaking. Different generation kinetics for these two kinds of defects were found through stretched-exponential-law analysis. The charged scattering centers can be formed from deep trapping or recombination centers through some relaxation processes.

The effects of deposition temperature and hydrogen dilution ratio an the transport properties of a-Si:H and a-SiC:H were investigated. Our results, together with previous results of other workers, indicate that for the a-Si:H films with increasing deposition temperature, the density of negatively charged defects increases and the density of positively charged and neutral defects decreases; and for the a-SiC:H films with increasing hydrogen dilution ratio, the density of positively charged, negatively charged, and neutral defects all shows a tendency to decrease. The photomixing technique, which can experimentally determine both the drift mobility and lifetime, together with subgap absorption, can provide information not only for the density of midgap defects, but also for the charge state profile of midgap defects.

Measurements of the electric field dependence of the drift mobility have indicated that an empirical relationship exists between the field dependence and the stability of a-Si:H. The great field dependence of mobility in annealed state indicates a poor stability upon light soaking.

Photoemission measurements to revealed inhomogeneities of composition or surface contaminates.

# Photomixing technique for separate determination of mobility and lifetime

We have developed a photomixing technique that allows us to determine both drift mobility and lifetime. This technique has been successfully applied to single crystalline, polycrystalline and amorphous semiconductors, such as c-Si,[1] a-Si:H,[2, 3] a-$As_2Te_3$,[4] polycrystalline $CuInSe_2$.[5] In the present paper we report *in situ* photomixing determination of lifetime and drift mobility in intrinsic hydrogenated amorphous silicon (a-Si:H) and hydrogenated amorphous silicon carbide (a-SiC:H) while light-soaking. We also present details of the theory and experimental setup of the photomixing technique.

The photomixing technique employed is based on the idea of heterodyne detection for photoconductors. When two similarly polarized monochromatic optical beams of slightly different frequencies are incident upon a photoconductor, the generation rate of electron-hole pairs and therefore the photocurrent produced, when a dc bias is applied, will contain components resulting from the square of the sum of the incident electrical fields. Consequently, a photocurrent composed of a dc and a microwave current due to the beat frequency of the incident fields will be produced; these two photocurrents allow a determination of the mobility and lifetime of the photo-generated carriers.

In the present work, instead of using two lasers, the multiple longitudinal modes of a single laser were used. In this case several microwave signals or photomixing signals with different frequencies can be generated due to the beating of the various laser longitudinal modes. Fig. 1 shows photomixing signals obtained with a Spectra-Physics 125A He-Ne laser (20 mW) on a commercial EG&G FND100 diode. The frequencies of the photomixing signals are: 84 MHz, 168 MHz, 252MHz,... 1.092 GHz. This is consistent with the fact that the frequencies ($f_m$) of the longitudinal modes of the laser are given by the following: $f_m = m\frac{c}{2L}$, where m is an integer, L is the length of the laser cavity and c is the speed of light in the cavity. The variation of the intensity of each frequency component is due to the intensity distribution of the laser modes and the frequency roll-off of the diode. The signal at 252 MHz was the one mostly used, since it has highest intensity.

The phenomenon of photoconductivity originates from the generation of electron-hole pairs to delocalized states by optical excitations. The electron-hole pair generation rate G is proportional to the square of the total electrical field (**E**) of the incident light, which is the superposition of the electrical fields ($\mathbf{E}_m$) of all the incident beams, i.e.,

$$\boldsymbol{E} = \sum_{m=1}^{l} \boldsymbol{E}_m exp(i\omega_m' t + i\phi_m), \quad (1)$$

where $\omega_m'$, $\phi_m$ are the angular frequency and the initial phase constant, respectively, of the $m^{th}$ optical beam (or mode), and $l$ is the total number of the optical beams (or modes).

If longitudinal modes of a laser are used, then

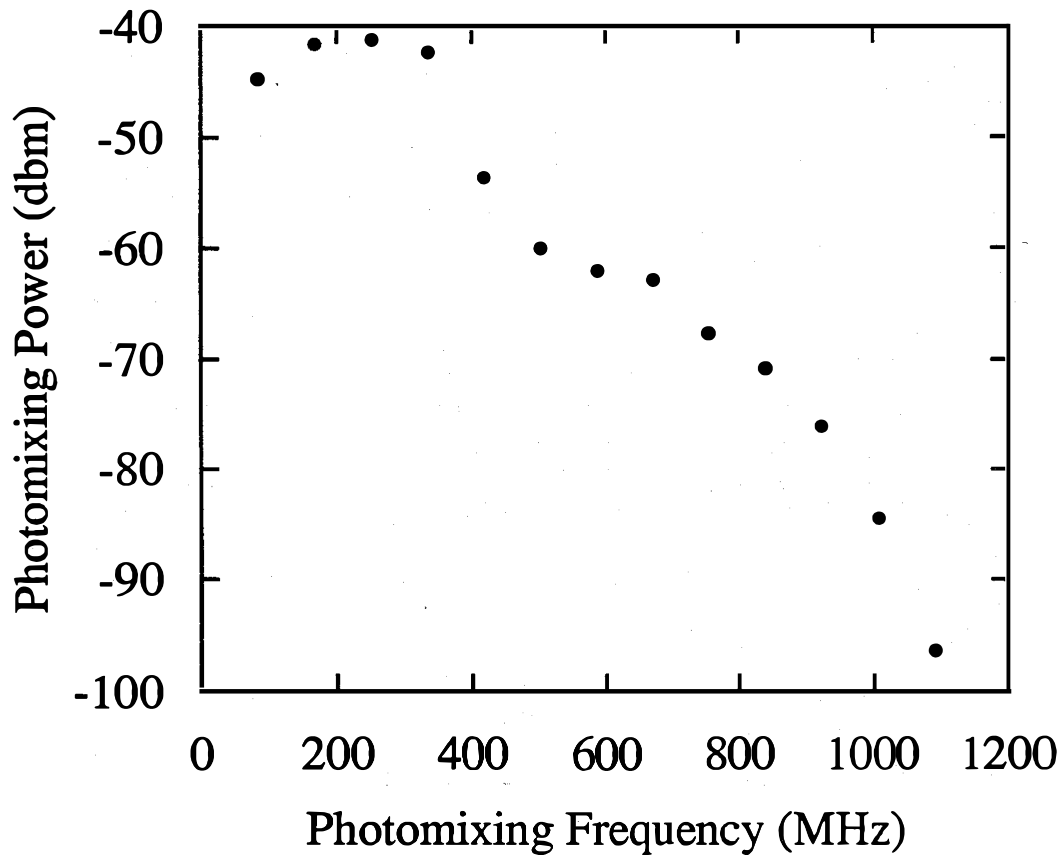


**Figure 1. Photomixing signals obtained with a commercial EG&G FND100 diode. The incident laser power was about 20 mW and the dc bias was 90 V (back biased). The frequencies of the photomixing signals are: 84 MHz, 168 MHz, 252MHz,... 1.092 GHz. The 252 MHz was the one mostly used, since it has highest intensity. 1 dbm = 1 mW.**

$$\omega_m' = \omega_1' + 2\pi(m-1)\frac{c}{2L} = \omega_1' + (m-1)\omega_0, \tag{2}$$

where $\omega_1'$ is the lowest frequency of the laser modes, m is an integer, L is the length of the laser cavity, and c is the speed of light in the cavity. For the Spectra-Physics 125 A laser used, $\omega_0 = 84$ MHz.

The total generation rate (G) and the generation rate of the mth optical beam (or mode) ($G_m$) are proportional to the square of the corresponding electrical field, i.e.: $G = C|\boldsymbol{E}|^2$ and $G_m = C|\boldsymbol{E}_m|^2$, where C is a proportionality constant.

The total generation rate G can be further expressed as:

$$\begin{aligned} G &= C\left|\sum_{m=1}^{l} \boldsymbol{E}_m exp\,(i\omega_m' t + i\phi_m)\right|^2 \\ &= C\sum_{m=1}^{l}|\boldsymbol{E}_m|^2 + 2CRe\left(\sum_{\substack{m=1 \\ (m>j)}}^{l}\sum_{j=1}^{l}\boldsymbol{E}_m\cdot\boldsymbol{E}_j exp\,[i(\omega_m' - \omega_j')t + i(\phi_m - \phi_j)]\right), \\ &= C\sum_{m=1}^{l}|\boldsymbol{E}_m|^2 + 2CRe\left(\sum_{m=1}^{l-1}\sum_{j=1}^{l-m}\boldsymbol{E}_m\cdot\boldsymbol{E}_j exp\,[i(\omega_{j+m}' - \omega_j')t + i(\phi_{j+m} - \phi_j)]\right) \end{aligned} \tag{3}$$

with $\boldsymbol{E}_{j+m}\cdot\boldsymbol{E}_j = |\boldsymbol{E}_{j+m}|\cdot|\boldsymbol{E}_j|\cos(\alpha_{j+m,j})$, where $\alpha_{j+m,j}$ is the angle between the two electric fields, which can also take into account the dynamic correlation between the two laser modes.

If longitudinal modes of a laser are used, then from Eq. (2): $\omega_{j+m}' - \omega_j' = m\omega_0 \equiv \omega_m$. Therefore, the total generation rate G can be rewritten as:

$$G = \sum_{m=1}^{l} G_m + 2Re\left(\sum_{m=1}^{l-1}\left(\sum_{j=1}^{l-m}\sqrt{G_{j+m}G_j}\cos(\alpha_{j+m,j})\,exp\,(i\phi_{j+m} - i\phi_j)\right)exp\,(i\omega_m t)\right). \tag{4}$$

The second term on the right hand side of the above equation has to be further evaluated, since the phase constants are unknown. First we evaluate the following quantity:

$$\left|\sum_{j=1}^{l-m}\sqrt{G_{j+m}G_j}\cos(\alpha_{j+m,j})\,exp(i\phi_{j+m}-i\phi_j)\right|^2$$

$$=\sum_{j=1}^{l-m}G_{j+m}G_j\cos^2(\alpha_{j+m,j}) \quad (5)$$

$$+2\sum_{j'=1}^{l-m}\sum_{\substack{j=1\\ i'>i}}^{l-m}\sqrt{G_{j'+m}G_{j'}G_{j+m}G_j}\cos^2(\alpha_{j+m,j})\cos(\phi_{j'+m}-\phi_{j'}+\phi_{j+m}-\phi_j)$$

For a laser without mode locking, the phase differences are random. Therefore, on the average, the second term on the right hand side of the above equation is much smaller than the first term and thus can be neglected to the first order. Consequently,

$$\sum_{i=1}^{l-m}\sqrt{G_{j+m}G_j}\cos(\alpha_{j+m,j})\,exp(i\phi_{j+m}-i\phi_j)=\sqrt{\sum_{j=1}^{l-m}G_{j+m}G_j\cos^2(\alpha_{j+m,j})}\,exp(i\delta_m), \quad (6)$$

where $\delta_m$ is a certain phase constant.

By defining $G_0=\sum_{m=1}^{l}G_m$ and $\lambda_m=\sqrt{\sum_{j=1}^{l-m}G_{j+m}G_j\cos^2(\alpha_{j+m,j})}/G_0$, and with the understanding that only the real part of the generation rate G should be considered, G can be rewritten as

$$G=G_0+2G_0\sum_{m=1}^{l-1}\lambda_m exp(i\omega_m t+i\delta_m). \quad (7)$$

$G_0$, the total dc generation rate, can be determined by the total power of the incident optical beams and can be measured by a conventional photodetector. $\lambda_m$, the effective modulation indices, can be determined by a Fabry-Perot interferometer. For a nearly linearly polarized laser beam, $\cos(\alpha_{j+m,j})\cong 1$.

In general, especially for amorphous semiconductors and insulators, there are four processes involved in the phenomenon of photoconductivity (Fig. 2): (1) photo-generation, (2) recombination, (3) trapping -- charge carriers are trapped to the localized states inside the band gap, (4) thermal emission -- trapped charge carriers are thermally emitted back to the extended states. The rate equation for photo-generated electrons, which are often the dominant carriers, in the conduction band in given by [2, 3, 6, 7]:

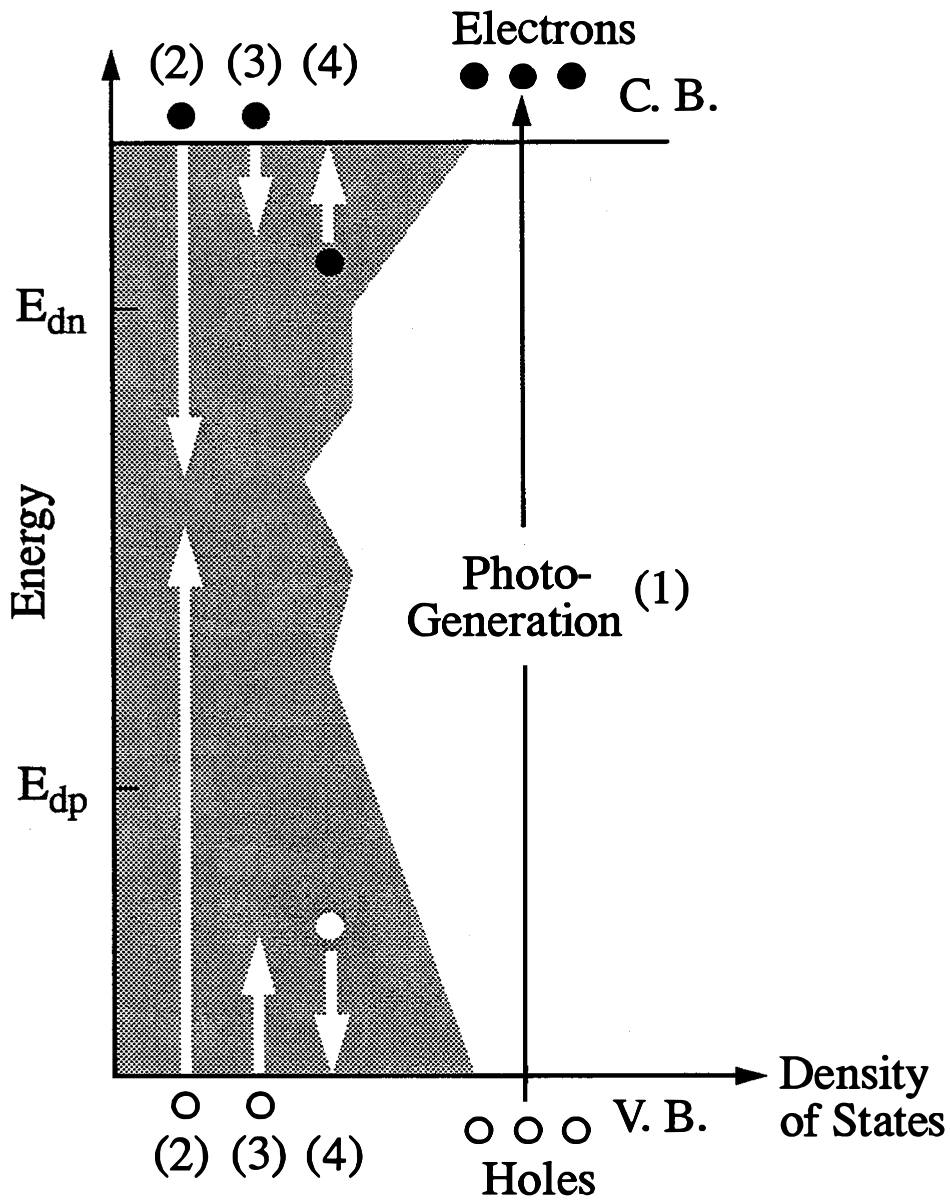


**Figure 2. Schematic diagram of the photo-generation (1), recombination (2), trapping (3) and thermal emission (4) processes. Only mono-molecular recombination is considered, since it is usually the recombination process with highest probability. $E_{dn}$ and $E_{dp}$ are demarcation energies for electrons and holes.**

$$\frac{dn}{dt} = G_0 + 2G_0 \sum_{m=1}^{l-1} \lambda_m exp\,(i\omega_m t + i\delta_m) - \int_0^{E_d} \frac{dn_T(E)}{dt} dE - \frac{n}{\tau_R}\,. \tag{8}$$

The first term on the right is the dc generation term, the second term is the ac generation from the beating of the various laser longitudinal modes with the difference frequencies of $\omega_m$, the integral describes the number of trapped electrons in localized states below the conduction band and above the electron demarcation level $E_d$ due to the trapping and thermal emission processes, and the last term represents the recombination of mobile electrons with trapped holes at a constant recombination rate $1/\tau_R$.

The trapped electron rate equation is given by[7]

$$\frac{dn_T(E)}{dt} = nK\,[N_T(E) - n_T(E)] - N_c K n_T(E)\, exp\left(-\frac{E}{kT}\right) \tag{9}$$

where $n_T(E)$ is the density of electrons in the localized states, $N_c$ is the effective number of states in the extended state transport band, $N_T$ is the density of states for the conduction band tail, K is the capture rate; the first term on the right represents the trapping and the second represents the thermal emission of electrons from localized gap states.

Exact solutions for Eqs. (8) and (9) can be obtained[6,7] in the form of $n = n_0 + \sum_{m=1}^{l-1} n_m exp\,(i\omega_m t)$ with $n_0 = \tau_R G_0$ and $n_m = \frac{2\lambda_m G_0}{\left(A^2 + B^2\right)^{1/2}} exp\,(i\phi_m)$, where, for simplicity the mixing frequency $\omega_m$ has been replaced by $\omega$,

$$A = \frac{1}{\tau_R} + \int_0^{a} \frac{D^2 K}{1 + exp\,[(E_{fn} - E)/kT]} \times \frac{exp\,[(E_{fn} - E)/(kT)]}{D^2 + \{1 + exp\,[(E_{fn} - E)/kT]\}^2} N_T(E)\, dE\,, \tag{10}$$

$$B = \omega \left| 1 + \frac{1}{n_0} \int_0^{E_d} \frac{exp\,[(E_{fn} - E)/kT]}{D^2 + \{1 + exp\,[(E_{fn} - E)/kT]\}^2} N_T(E)\, dE \right|, \tag{11}$$

and $D = \frac{\omega}{N_c K exp\,(-E_{fn}/kT)}$, $E_{fn} = kT ln\,(N_c/n_0)$, and $E_\omega = kT ln\,(N_c K/\omega)$.

In the above equations $E_{fn}$ is the quasi-Fermi level for electrons and $E_\omega$ is a frequency-dependent demarcation energy. Their physical meanings become clear if we rewrite the last two of the above equations as $n_0 = N_c exp(-E_{fn}/kT)$ and $\omega = N_c K exp(-E_\omega/kT)$ .

Thus, roughly speaking, above $E_\omega$ the carriers are in quasi-thermal equilibrium since their thermal emission frequencies are higher than the mixing frequency $\omega$, while those below $E_\omega$ are in deep traps with concomitant emission frequencies less than the mixing frequency $\omega$.

When a dc bias is applied, the resulting dc and root-mean-square ac conductivities are given by [2]

$$\sigma_{dc} = eG_0\mu_0\tau_R, \tag{12}$$

$$\sqrt{\langle\sigma_{ac}^2\rangle} = \sqrt{2}eG_0\mu_0\frac{\lambda}{\sqrt{A^2+B^2}}. \tag{13}$$

In the case of no trapping, the above equation becomes

$$\sqrt{\langle\sigma_{ac}^2\rangle} = \sqrt{2}eG_0\mu_0\frac{\lambda}{\sqrt{\omega^2+1/\tau_R^2}}. \tag{14}$$

Comparing the last two equations, one can see that in general the quantity $\mu_0\frac{\sqrt{\omega^2+1/\tau_R^2}}{\sqrt{A^2+B^2}}$ plays the same role in the case of trapping as the extended state mobility $\mu_0$ in the case of no trapping, thus the former can be identified as an effective mobility or drift mobility ($\mu_d$), i.e.,

$$\mu_d = \mu_0\frac{\sqrt{\omega^2+1/\tau_R^2}}{\sqrt{A^2+B^2}} \tag{15}$$

For our photomixing frequency of 252 MHz, $\omega$ is about 1.58 GHz (corresponding to a time scale of 630 ps). Since the recombination lifetime $\tau_R$ is usually greater than 10 ns, thus $\omega^2\tau_R^2 >> 1$, therefore the above equation can be simplified to

$$\mu_d = \mu_0\frac{\omega}{\sqrt{A^2+B^2}}. \tag{16}$$

From Eqs. (13) and (16) one can see that the drift mobility ($\mu_d$) is an experimentally measurable quantity with no need for any detailed knowledge of trapping and thermal emission, i.e.:

$$\mu_d = \omega\sqrt{\langle\sigma_{ac}^2\rangle}/\left(\sqrt{2}eG_0\lambda\right), \tag{17}$$

where $\lambda$ (= 7.05%) is an effective modulation index. Attention is focused on electrons, since they have more dominant contributions to transport in intrinsic a-Si:H and a-SiC:H samples than holes.

The root-mean-square ac photoconductivity $\sqrt{\langle\sigma_{ac}^2\rangle}$ was determined through the measurement of the power of the ac or photomixing signal using a Tektronix 492P spectrum analyzer. The drift mobility $\mu_d$ can thus be obtained from Eq. (17) and the lifetime $\tau$ corresponding to $\mu_d$ can be written as

$$\tau = \frac{\mu_0\tau_R}{\mu_d} = \frac{\sigma_{dc}}{eG_0\mu_d}. \tag{18}$$

The photomixing process for single crystalline materials is a special case of the above discussion such that the trapping term in Eq. (8) can be set to zero. In this case, the integrals in the Eqs. (10) and (11) are zero, and Eqs. (17) and (18) give the drift mobility $\mu_d$ which is equal to the extended state mobility $\mu_0$ and the recombination lifetime $\tau_R$ respectively. In the case of amorphous or polycrystalline materials, the drift mobility $\mu_d$ usually is less than the extended state mobility $\mu_0$, but approaches to $\mu_0$ at high frequency or high temperature limit according to Eqs. (10) and (11).

The absolute values for mobility and lifetime can be obtained through the measurement of the absolute values of the microwave photomixing signal and the generation rate.

To see the temperature dependence of the transport properties under trapping, one can use the following approximations for A and B in Eq. (16): $A \approx \frac{1}{\tau_R} + \int_{E_\omega}^{E_{fn}} KN_T(E)\,dE$, $B \approx \omega + \frac{\pi}{2}kTKN_T(E_\omega)$, if D >> 1 or the frequency-dependent demarcation energy $E_\omega$ is well above the quasi-Fermi level $E_{fn}$, which is true in our case. Therefore, further considering that the recombination effect (the $1/\tau_R$ term in the expression for A) can be proven to be negligible:

$$\mu_d = \mu_0 \frac{\omega}{\sqrt{\left[\omega + \frac{\pi}{2}kTKN_T(E_\omega)\right]^2 + [\varepsilon K N_T(E_\omega)]^2}}$$

$$= \mu_0 \frac{\omega}{\sqrt{\left[\omega / [KN_T(E_\omega)] + \frac{\pi}{2}kT\right]^2 + \varepsilon^2 K g_c}} exp\left(kT\frac{ln(N_c K/\omega)}{\varepsilon}\right), \qquad (19)$$

where the distribution of tail states is given by: $N_T = g_c exp(-E/\varepsilon)$, and $g_c$ is the density of states in the conduction band and $\varepsilon$ is the spread of the band tail.

Thus by measuring the dc and the ac photoconductivities at a single photomixing frequency as a function of temperature, $\mu_0$, K and $\varepsilon$ can be determined through curve fitting according to Eq. (19). The recombination lifetime $\tau_R$ is then given by: $\tau_R = \frac{\sigma_{dc}}{eG_0\mu_0}$.

It is interesting to point out that when $\varepsilon > kT$ and the photomixing frequency is much less than certain "trapping frequencies", i.e., $\omega \ll \frac{\pi}{2}kTKN_T(E_\omega)$ and $\omega \ll \varepsilon KN_T(E_\omega)$, explicit dispersive transport can be obtained from Eq. (19): $\mu_d \propto \omega^{1-kT/\varepsilon}$.

## Experimental setup of photomixing

The block diagram of the experimental setup for photomixing is shown in Fig. 3. The dc photo-signal was measured by a Keithley 617 Programmable Digital Electrometer, and the photomixing signal, i.e., the ac photo-signal, was measured by a Tektronix 492P Spectrum Analyzer with a frequency range of 50 KHz to 220 GHz. The dc and the ac signals were separated by a low pass filter and a high pass filter, which are incorporated in a bias tee, that was connected to a three stub tuner. By tuning the stub tuner, the reflection of the photomixing signal, which is in the microwave range, from the Spectrum Analyzer can be reduced to nearly zero, and thus the true measurements of the photomixing signal can be achieved. All the equipment were controlled by an IBM PC through a National Instruments Lab-PC card.

Measurements in the temperature range from 80 K to 330 K were performed with a Janis double vacuum jacket dewar (model 8 DT) and a Lake Shore temperature controller (model DRC 80C). Measurements from 150 K to 450 K were performed with a vacuum dewar and a software emulated temperature controller constructed in house.

The light sources used for photomixing and light soaking are included in the optical setup, the details of which are show in Fig. 4.

A Spectra-Physics 125A He-Ne laser was used as the light source for photomixing, and a 600 W or a 1000 W tungsten halogen lamp was used as the light source for light soaking measurements. In ordinary

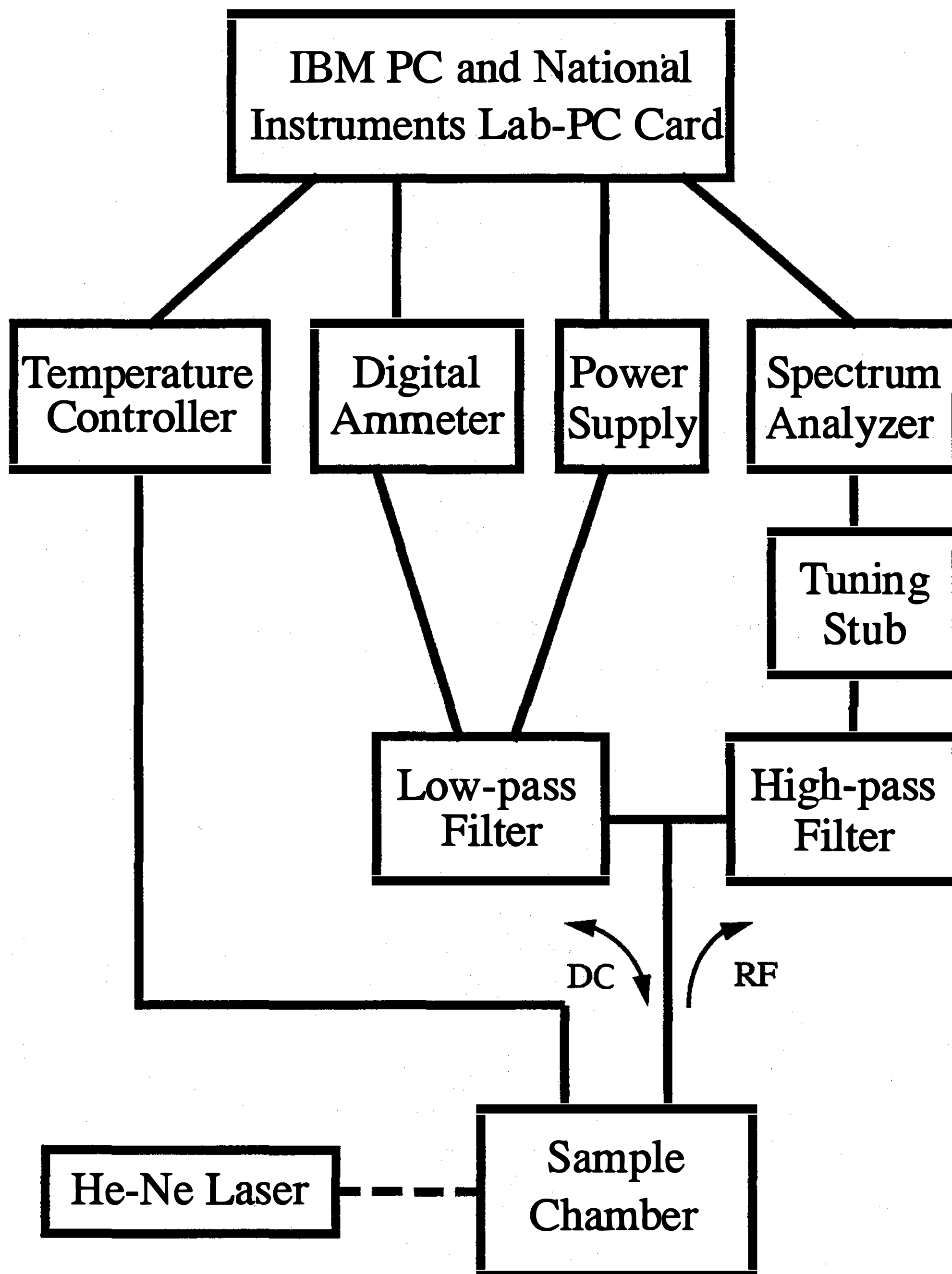


**Figure 3. Block diagram of the experimental setup for photomixing.**

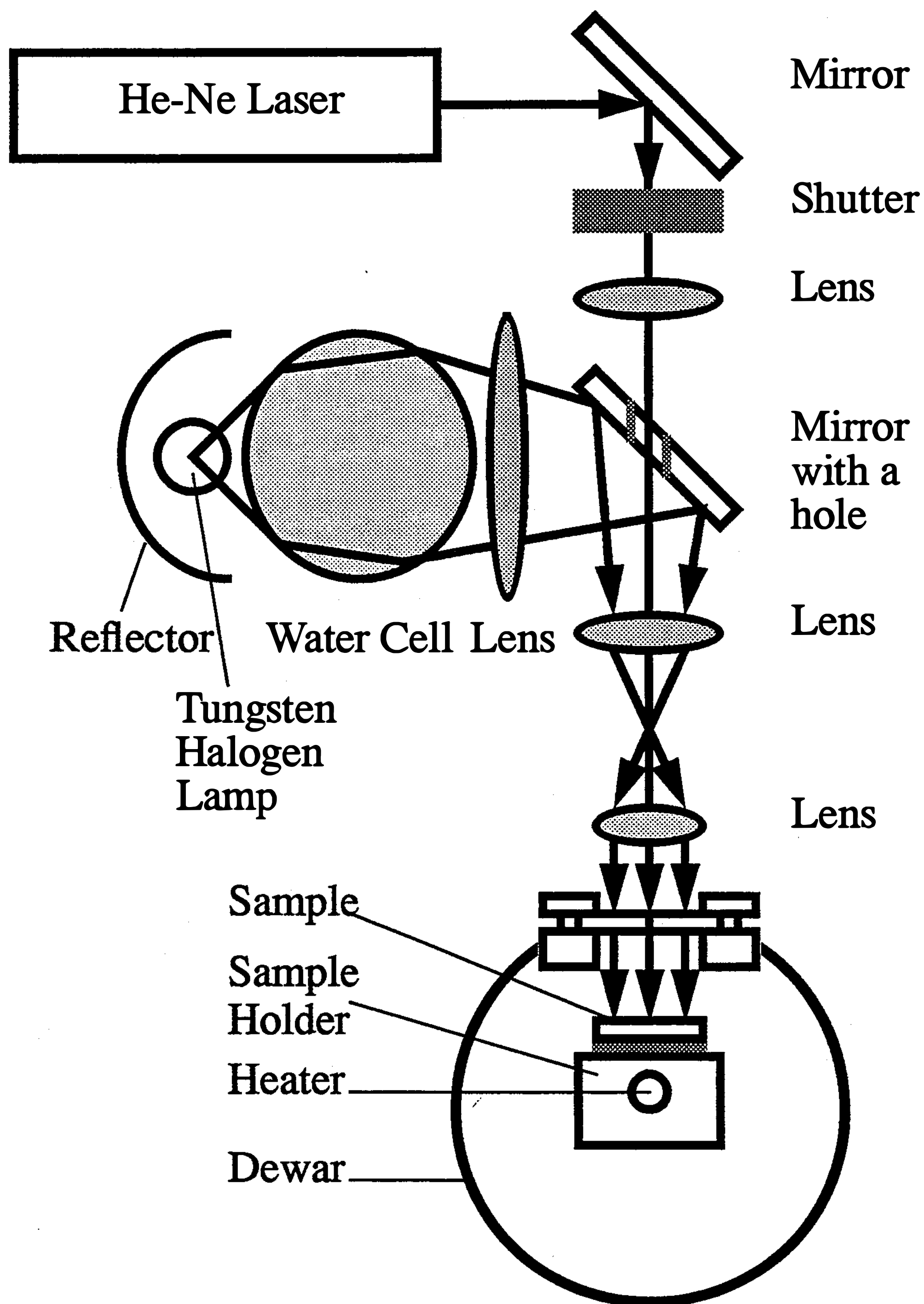


**Figure 4. The optical setup for photomixing and light soaking.**

photomixing measurements the tungsten halogen lamp was turned off, only the laser beam was focused onto the sample. In light soaking measurements, the light from the tungsten halogen lamp was focused onto the sample, the laser beam can also be focused onto the sample for photomixing measurements *in situ* with light soaking. In this case the light from the lamp and the laser beam were combined together by a mirror with a hole in the middle.

# Result and analysis

### Continuous decay of drift mobility in intrinsic a-Si:H and a-SiC:H upon light soaking investigated by the photomixing technique

The intrinsic a-Si:H, provided by the National Renewable Energy Laboratory (NREL), was deposited by glow discharge on Corning 7059 glass at a substrate temperature of 250 C. The sample was 1. 3 μ thick with co-planar chromium contacts. The hydrogen content was about 10%. Measurements were performed at room temperature. The sample was annealed for a few hours before the measurements. The light source for light soaking was a Tungsten Halogen lamp yielding a light intensity of about 2.5 sun at the sample surface and the photomixing signal was obtained by using a He-Ne laser (632.8 nm).

Fig. 5 a-d show the dc photoconductivity $\sigma_{dc}$, power of the photomixing signal $P_{mix}$, lifetime $\tau$ and drift mobility $\mu_d$ for the intrinsic a-Si:H sample versus light soaking time. In addition to the decay of the dc photoconductivity and lifetime, continuous decay of the drift mobility can be seen due to light soaking, which reveals a new phenomenon for the Staebler-Wronski effect.

For intrinsic a-Si:H the drift mobility is determined by the trapping of electrons into the conduction band tail and the scattering of electrons by the intrinsic disorder. Both enhanced trapping and scattering can result in the decay of the drift mobility. A question of interest is: which one is the dominant mechanism for the decay of the drift mobility upon light soaking.

The concentration of defects generated by light soaking is usually about $10^{16}cm^{-3}$ for dangling bonds, located near the mid-gap, at saturation level [8] and about $10^{18}cm^{-3}$ for the light induced defects in the valence band tail[9]. Thus it is conceivable that the conduction band tail, with integrated concentration of states of $10^{19}cm^{-3}$, would not be altered by these defects, especially since the frequency dependent demarcation energy $E_\omega$ for the photomixing process is about 0.1 eV below the conduction band edge,[2, 3] where the density of states for the conduction band tail is high ($\sim10^{20}cm^{-3}eV^{-1}$). Therefore the enhanced scattering has to be the dominant mechanism for the light induced decay of the drift mobility. In order for the light generated defects ($\sim10^{18}cm^{-3}$) to compete with the intrinsic neutral scatters due to disorder ($\sim10^{22}cm^{-3}$) of much greater population so as to reduce the drift mobility, part of the light generated defects can be charged so that they can have much greater scattering cross sections and may form long-range potential fluctuations. Without significant changes for trapping, the lifetime $\tau$ and the drift mobility $\mu_d$ are thus proportional to the recombination lifetime $\tau_R$ and the extended state mobility $\mu_0$. Therefore

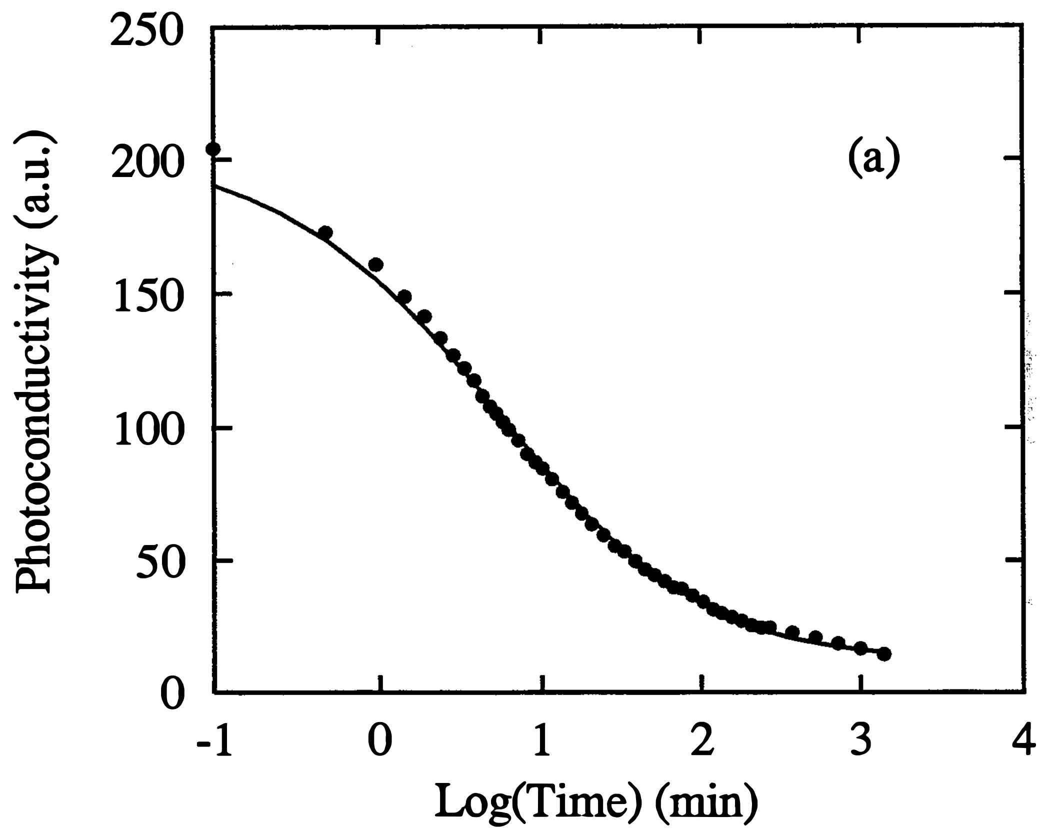


**Figure 5 (a). The dc photoconductivity $\sigma_{dc}$ for the intrinsic a-Si:H sample versus light soaking time. The solid line is curve fit to the stretched exponential law (Eq. (22)).**

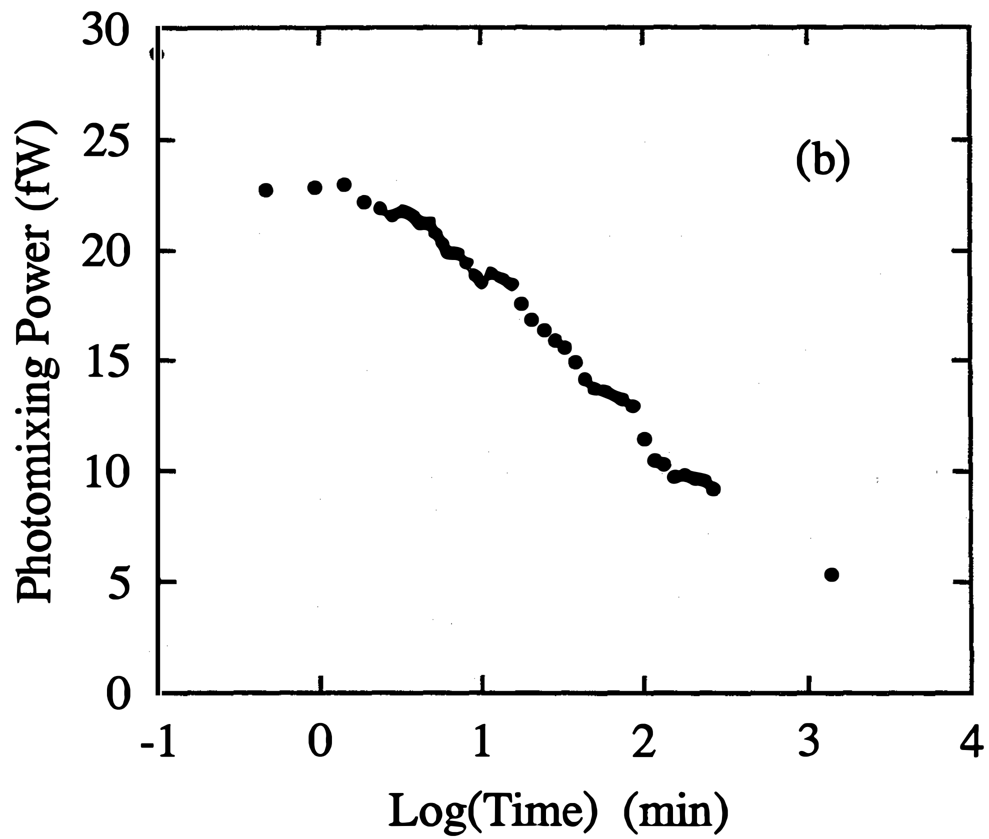


**Figure 5 (b). Power of the photomixing signal $P_{ml=5}$ for the intrinsic a-Si:H sample versus light soaking time.**

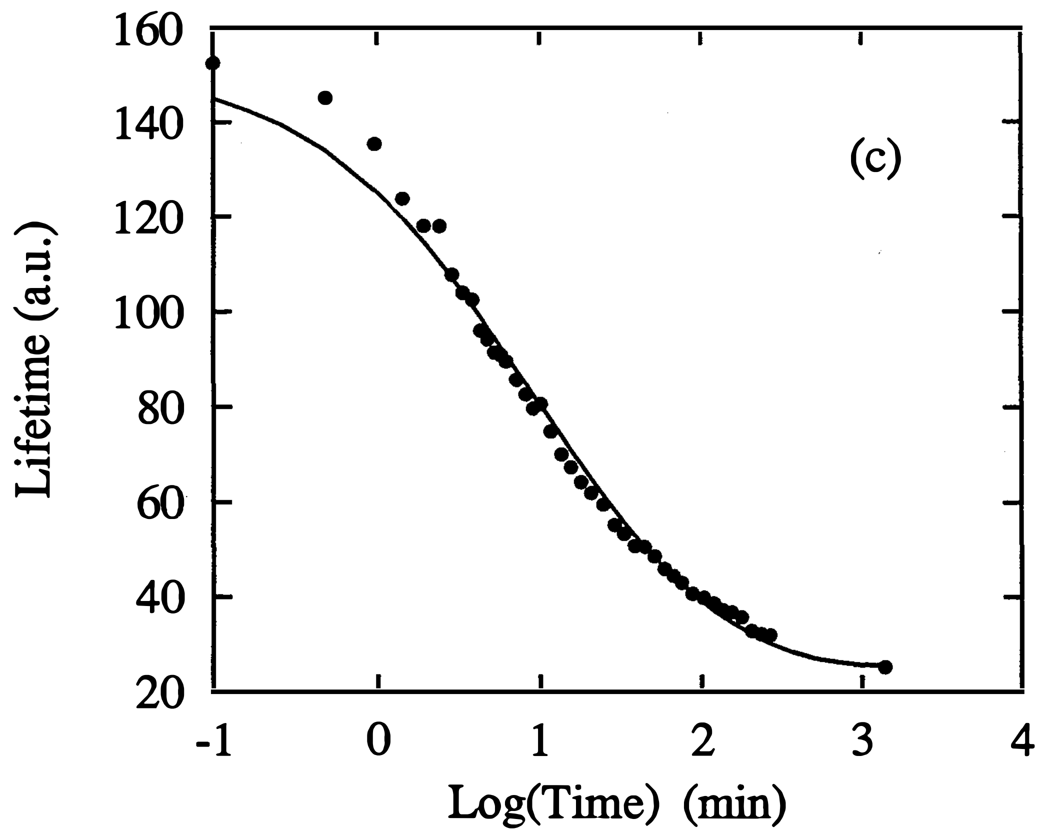


**Figure 5 (c). The lifetime $\tau$ for the intrinsic a-Si:H sample versus light soaking time. The solid line is curve fit to the stretched exponential law (Eq. (22)).**

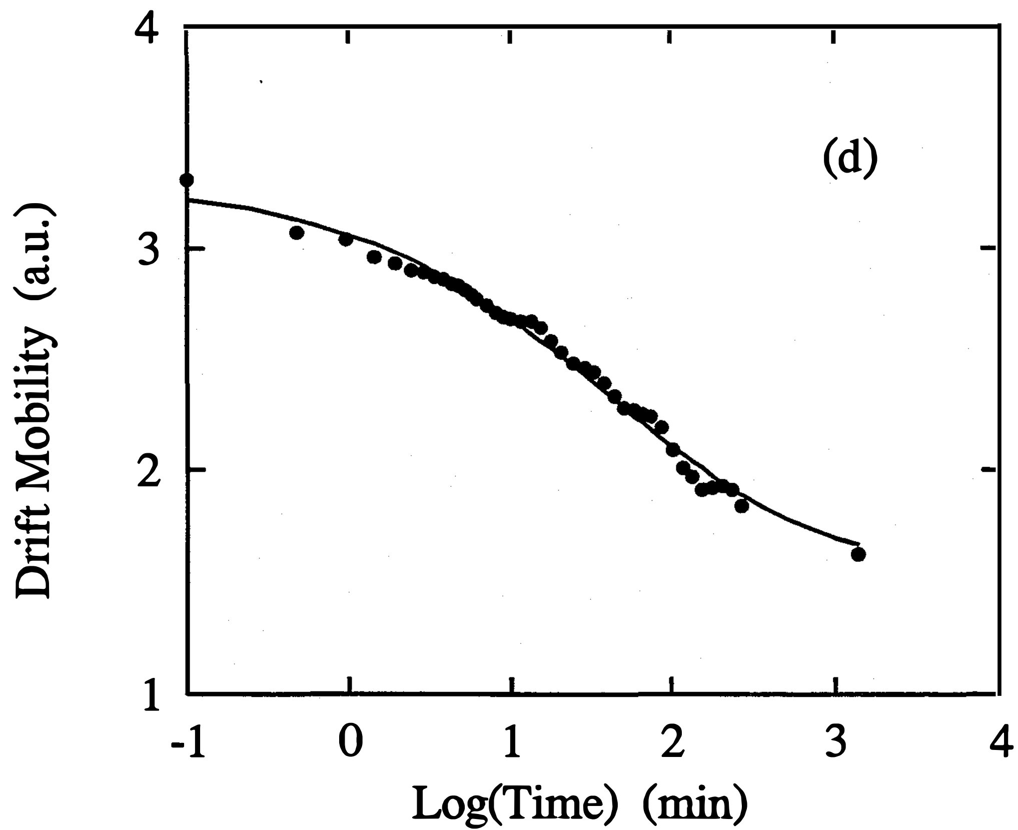


**Figure 5 (d). The drift mobility $\mu_d$ for the intrinsic a-Si:H sample versus light soaking time. The solid line is curve fit to the stretched exponential law (Eq. (22)). In addition to the decay of the dc photoconductivity and lifetime, continuous decay of the drift mobility can be seen due to light soaking. Different stretched exponential parameters were found, which are shown in Table I. The drift mobility $\mu_d$ was determined by Eq. and $\sqrt{\langle \sigma_{ac}^2 \rangle}$ was determined by $P_{mix}$.**

$$\frac{1}{\tau} \propto \frac{1}{\tau_R} = N_r s_r v , \tag{20}$$

$$\frac{1}{\mu_d} \propto \frac{1}{\mu_0} \propto N_s s_s v , \tag{21}$$

where $N_r$, $N_s$ are the effective concentrations of the recombination and the scattering centers, $s_r$, $s_s$ are the effective recombination and scattering cross sections, and v is the thermal velocity of charge carriers.

The solid lines in Fig. 5 are curve fit to the following stretched exponential law:

$$N = N_s - (N_s - N_0) \, exp \, [-(t/\tau_0)^{\beta}] , \tag{22}$$

by replacing N with $1/\sigma_{dc}$, $1/\tau$ and $1/\mu_d$ respectively, where N is the defect concentration at time t, $N_0$ and $N_s$ are the initial and saturated defect concentrations, $\beta$ is the stretching parameter, and $\tau_0$ is the time constant. The results from curve fit are listed in Table I.

**Table I.** Summary of results from the curve fit for a-Si:H.

| | $\beta$ | $\tau_0$ (min) |
|---|---|---|
| From dc Photoconductivity | 0.65 | 300 |
| From Lifetime | 0.64 | 130 |
| From Drift Mobility | 0.49 | 160 |

As can be seen from the above table, different stretched-exponential parameters for photoconductivity, lifetime and drift mobility were obtained, which indicates the generation of defects with different generation kinetics upon light soaking. Our studies so far do not reject any existing microscopic models[10, 11, 12-17] for the Staebler-Wronski effect, such as weak bond breaking [12-15] and charge trapping [16] models. Rather our studies indicate that combinations of different models may be necessary to explain the generation of defects with different characteristics. The recombination centers for electrons are most likely positively charged or neutral defects, whereas the scattering centers for electrons can be either negatively or positively charged defects. Upon light soaking, in addition to the generation of defects, the defects that serve as deep trapping or recombination centers can be charged, since electrons and holes are trapped to them. This results in enhanced scattering and thus the decay of the drift mobility for electrons. The charged defects may become quasi-stable through some relaxation processes and can also form certain long-range potential fluctuations,[18-22] if they are not spatially correlated.

All the above statements are also supported by the light soaking experiments on the a-SiC:H sample. Decay of photoconductivity lifetime and drift mobility upon light soaking were found (Fig. 6 a-c). The solid lines are the curve fit according to the stretched exponential law. The increase for the drift mobility at

t ~ 100 min during light soaking is probably due to an increase of the sample temperature upon light illumination. Table II shows the results from the curve fit according to the stretched exponential law (Eq. (22)). Different parameters were found for different decay processes.

It should be pointed out that in some Time-Of-Flight (TOF) measurements the decay of drift mobility due to light soaking was not found.[23-25] This basically results from the facts that the photomixing process is a fast process with an equivalent time scale of 630 ps and is close to the steady state limit, since the ac generation rate is only about 14% of the total generation rate, which allow it to study the transport of electrons about 0.1 eV below the conduction band edge.[2, 3] Therefore, the photomixing measurements are very sensitive to changes in the extended state transport path, such as the change in the profile of scattering centers and long-range potential fluctuations, whereas on the other hand, the drift mobility measured by TOF, which is a slower process with a time scale of about 10 ns, is mainly limited by the trapping and thermal emission processes and thus may not be sensitive to changes in the extended state transport path.

**Table II.** Summary of results from the curve fit for a-SiC:H.

| | $\beta$ | $\tau_0$ (min) |
|---|---|---|
| From dc Photoconductivity | 0.87 | 200 |
| From Lifetime | 0.93 | 170 |

### Effects of deposition conditions on transport properties of intrinsic a-Si:H and a-SiC:H films investigated by the photomixing technique

Extensive studies on effects of the deposition conditions, such as deposition temperature ($T_s$)[26-31] and hydrogen dilution ratio (R),[32,33] on the structural and electronic properties of a-Si:H and a-SiC:H films have been performed in attempt to improve the quality of these films for solar cell applications.[26-33] The experimentally available transport data for these films, however, are normally limited to conductivities and $\mu\tau$ products which are convolutions of a few separate physical parameters. With the unique advantage of the photomixing technique of being able to experimentally determine both the drift mobility ($\mu_d$) and lifetime ($\tau$), we report here the drift mobility (at 480 K), lifetime (at 480 K) and the Urbach energy ($\varepsilon$) of a-Si:H and a-SiC:H films as a function of deposition temperature ($T_s$) and hydrogen dilution ratio (R), respectively.

$$\mu_d = \omega\sqrt{\langle\sigma_{ac}^2\rangle}/\left(\sqrt{2}eG_0\lambda\right) \tag{23}$$

$$\tau = \sigma_{dc}/(eG_0\mu_d) \tag{24}$$

where $\omega$ is the photomixing angular frequency (~ 1.58 GHz, corresponding to a time scale of ~ 630 ps), $\lambda$ (~ 7.05%) is an effective modulation index, $G_0$ is the dc electron-hole pair generation

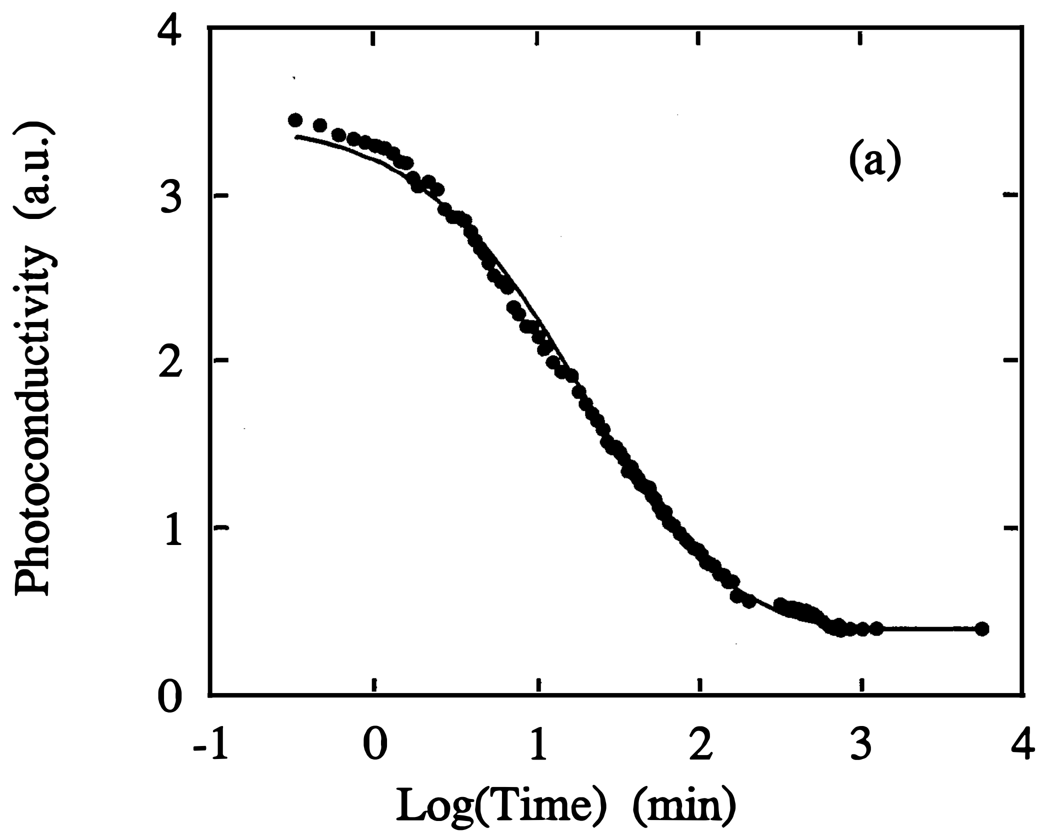


**Figure 6 (a). Thedc photoconductivity $\sigma_{dc}$ for the a-SiC:H sample versus light soaking time. The solid line is curve fit to the stretched exponential law (Eq. (22)).**

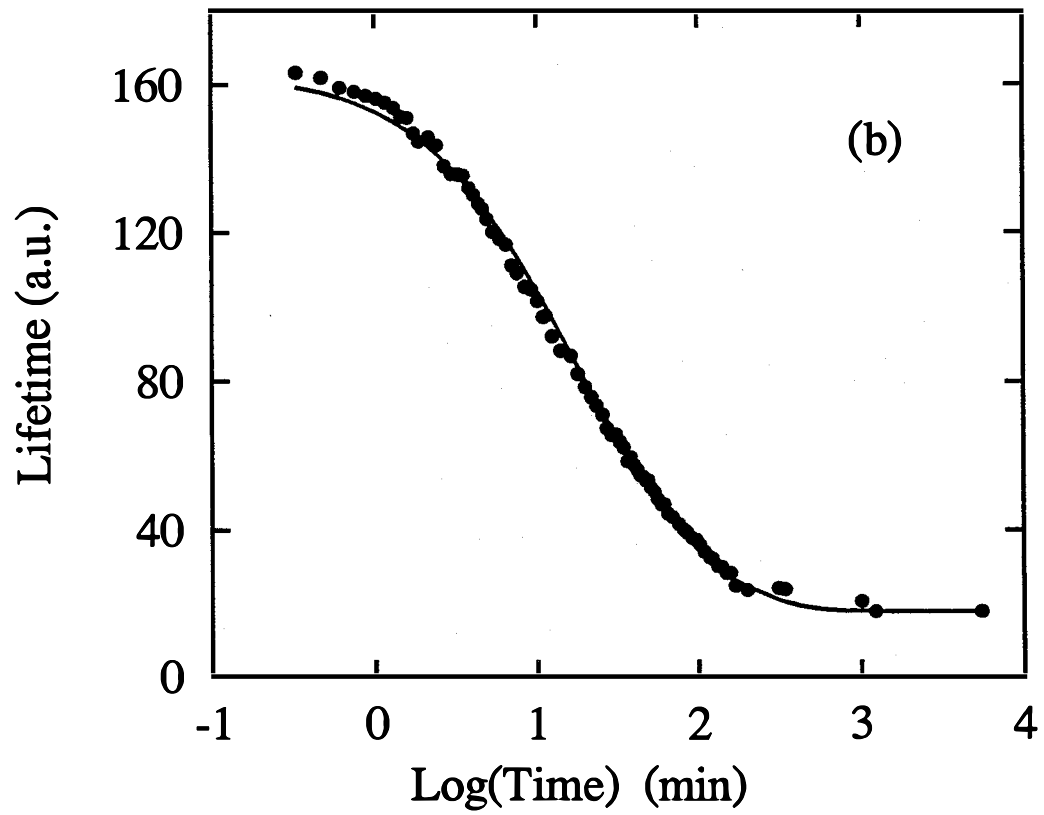


**Figure 6 (b). The lifetime $\tau$ for the a-SiC:H sample versus light soaking time. The solid line is curve fit to the stretched exponential law (Eq. (22)). Different stretched exponential parameters were found, which are shown in Table II.**

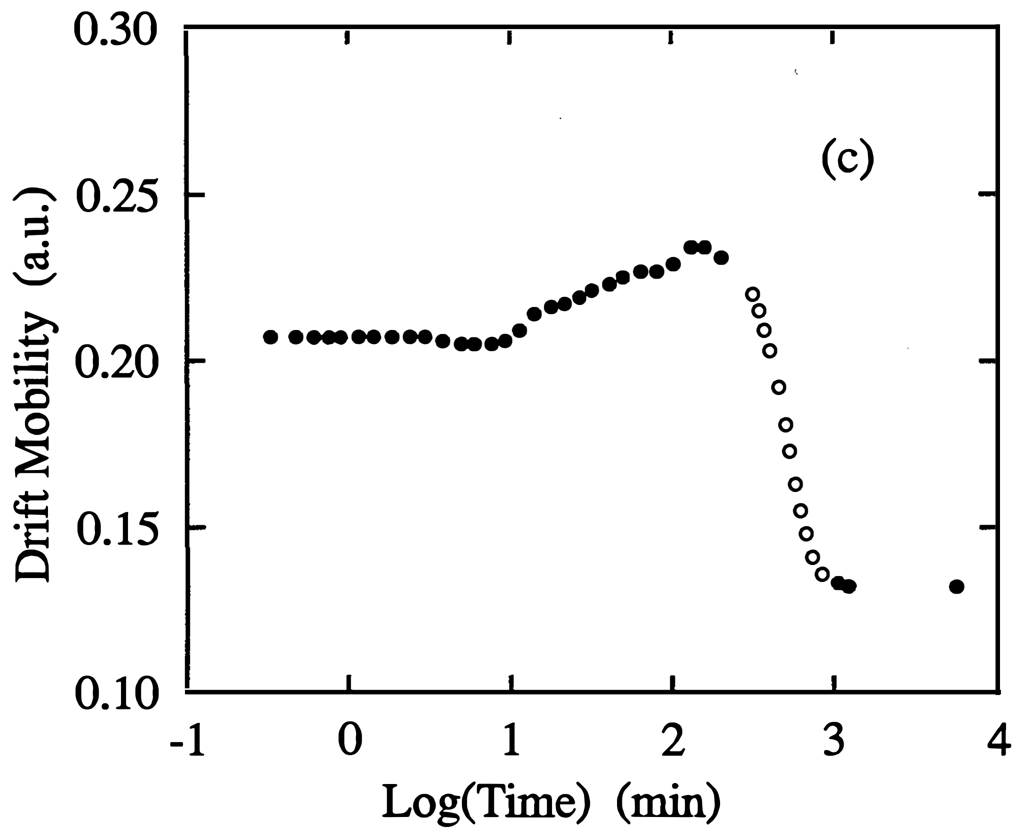


**Figure 6 (c). The drift mobility $\mu_d$ for the a-SiC:H sample versus light soaking time. In addition to the decay of the dc photoconductivity and lifetime, decay of the drift mobility can be seen due to light soaking. The increase for the drift mobility at t ~ 100 min during light soaking is probably due to an increase of the sample temperature upon light illumination and the open circles for the drift mobility were obtained from the dc photoconductivity and curve-fitted lifetime data.**

rate, $\sigma_{dc}$ is the dc photoconductivity, and $\sqrt{\langle \sigma_{ac}^2 \rangle}$ is the root-mean-square ac photoconductivity which is determined by the power of the microwave photomixing signal. The Urbach energy ($\varepsilon$) is determined by curve-fitting to the drift mobility data as a function of the measurement temperature.

The intrinsic a-Si:H films[29-31] were prepared by RF glow discharge at deposition temperatures ($T_S$) of: 200 C, 220 C, 240 C, 265 C, and 280 C. The a-SiC:H films[32,33] were prepared by RF glow discharge with hydrogen dilution ratio ($R = H_2/(CH_4+SiH_4)$) of: 0 ($T_S$ = 250 C), 20 ($T_S$ = 250 C), and 25 ($T_S$ = 305 C). Most of these samples were provided and fully characterized by the Wronski group at Penn. State University.[29-33]

For the a-Si:H films with increasing deposition temperature ($T_S$), the lifetime (at 480 K) increases (Fig. 7), the drift mobility (at 480 K) decreases (Fig. 8), and the Urbach energy decrease, except for the sample with $T_S$ = 200 C (Fig. 9). The decrease of the Urbach energy (Fig. 9) indicates that the Urbach edges get sharper and the atomic structure of the films gets closer to that of crystalline Si. This is consistent with previous results indicating that the monohydride and dihydride content, and the void fraction all decrease with increasing deposition temperature.[31] The $\mu\tau$ product (at 480 K) of these films increases as the deposition temperature ($T_S$) increases to 240 C, and converges to a constant value at higher $T_S$. This is also consistent with previous results.[31]

It is important to note that the decrease of the monohydride and dihydride content, and the void fraction in these a-Si:H films as a result of increasing deposition temperature ($T_S$) actually results in an increase in the subgap absorption, i.e., higher density for the midgap defects.[31] Nevertheless, the lifetime for electrons (as they are the dominant photoconductive charge carriers in intrinsic a-Si:H films) still increases with increasing $T_S$ (Fig. 7). All these indicate that with increasing deposition temperature ($T_S$), the density of defects with relatively large deep trapping and recombination cross sections for electrons, such as positively charged and neutral defects, must decrease, whereas the density of defects with relatively small deep trapping and recombination cross sections for electrons, such as negatively charged defects, must increase to account for the increase of the subgap absorption. The increase of charged defects with increasing $T_S$ is also evidenced by the decrease of the drift mobility (Fig. 8), as the charged defects can enhance the scattering of electrons, especially if they form certain long range potential fluctuations.[18-22] In other words, the change in the deposition temperature ($T_S$) not only affects the density of midgap defects, but also, more importantly, affects the charge state profile of midgap defects.

For the a-SiC:H films with increasing hydrogen dilution ratio, both the lifetime (at 480 K) (Fig. 10) and the drift mobility (at 480 K) (Fig. 11) increase, and the Urbach energy shows a tendency to decrease (Fig. 12). These results are consistent with previous results indicating that with increasing hydrogen dilution ratio, both the voids fraction and the density of midgap defects decreases,[32,33] and further indicate that the density of positively charged, negatively charged, and neutral defects all shows a tendency to decrease with increasing hydrogen dilution ratio.

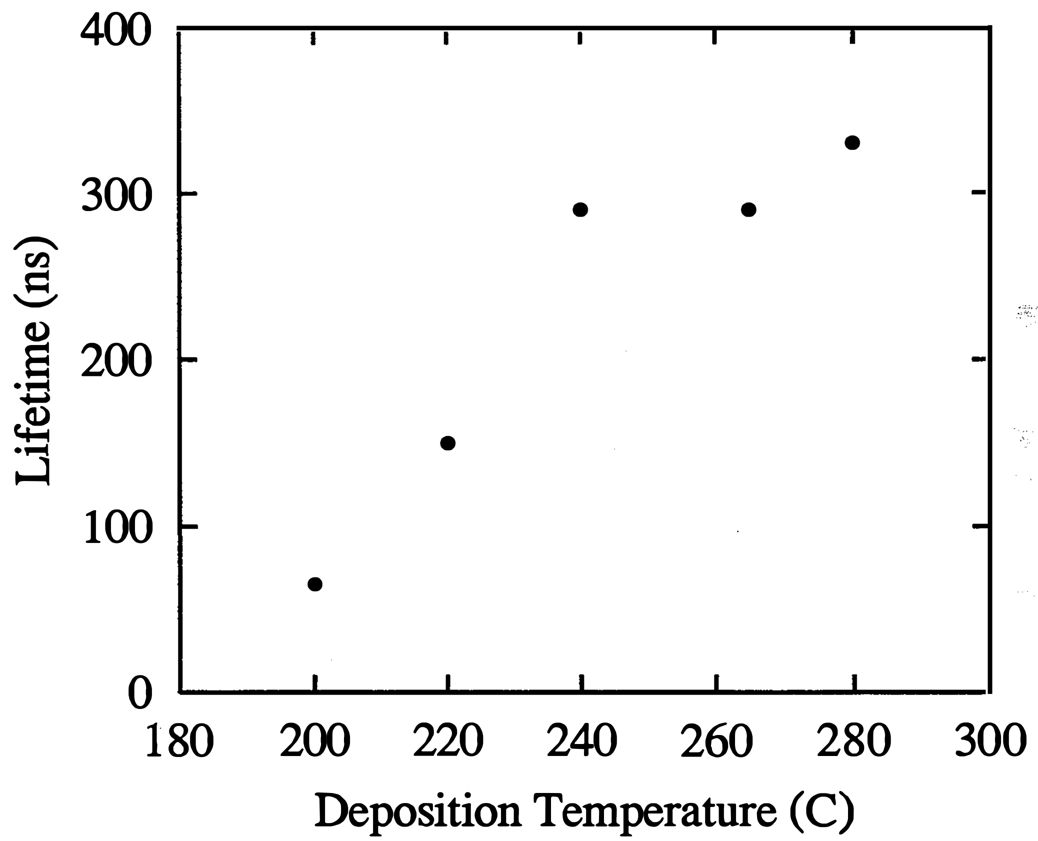


**Figure 7. Lifetim (at 480 K) of a-Si:H films as a function of deposition temperature.**

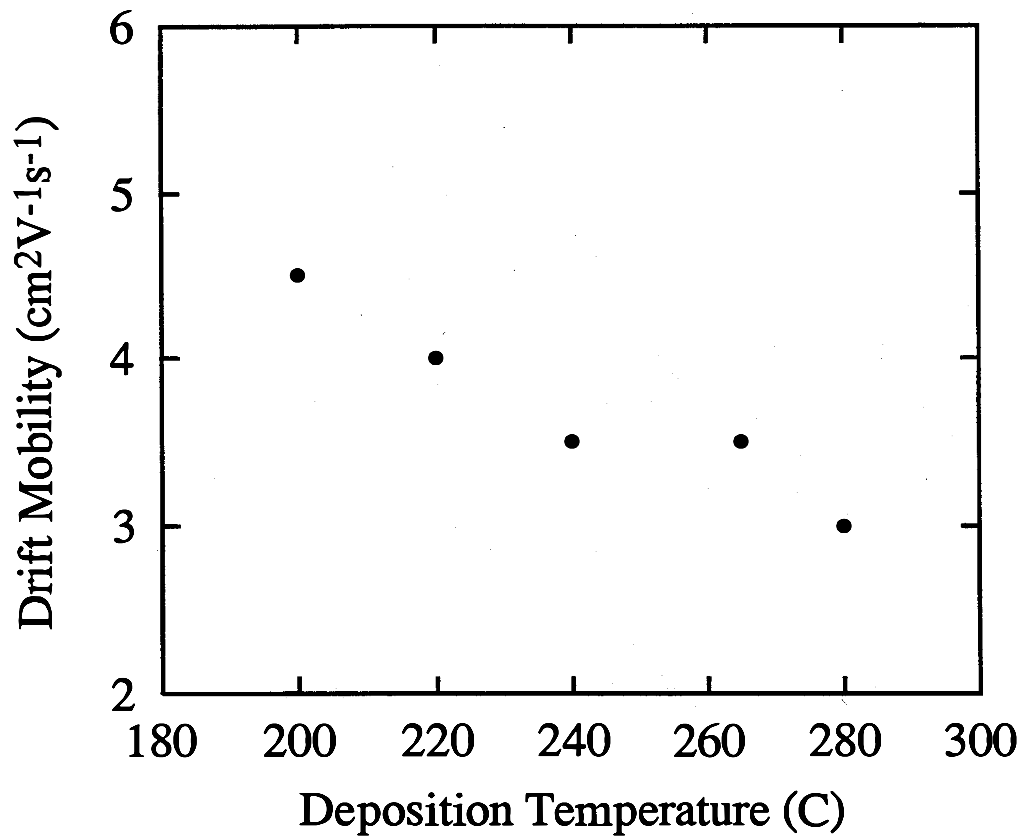


**Figure 8. Drift Mobility (at 480 K) of a-Si:H films as a function of deposition temperature.**

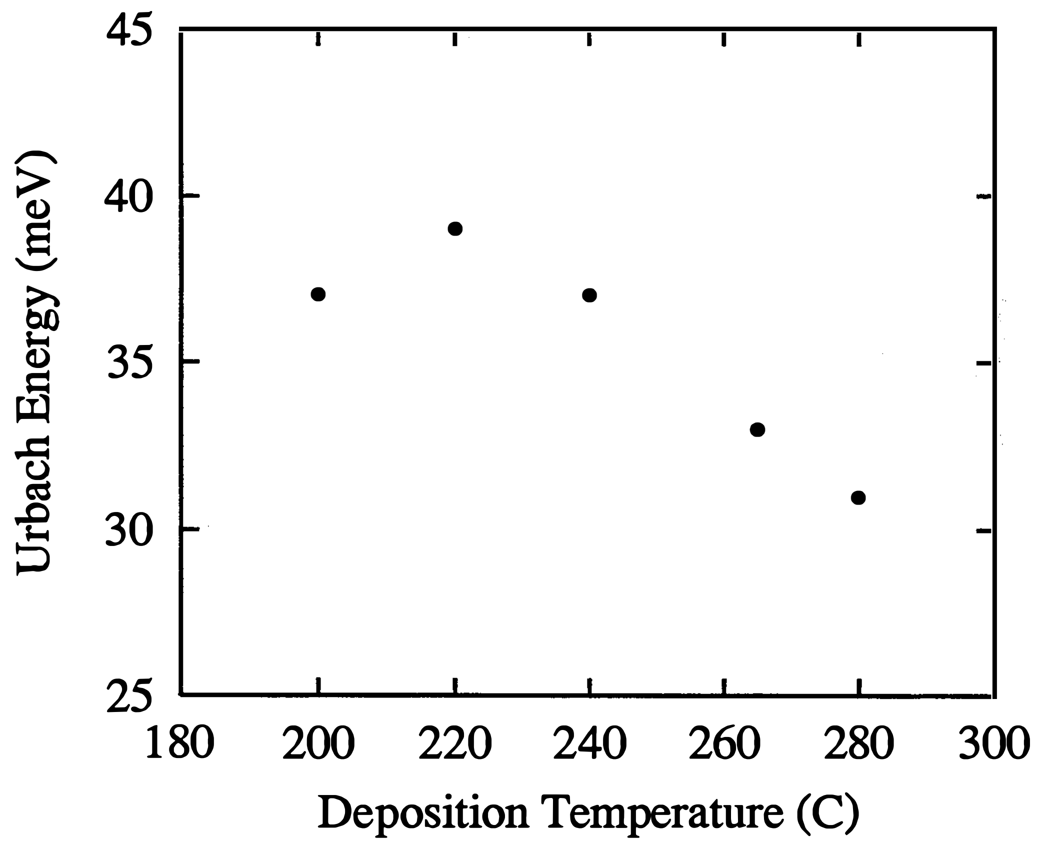


**Figure 9. Urbach energy of a-Si:H films as a function of deposition temperature.**

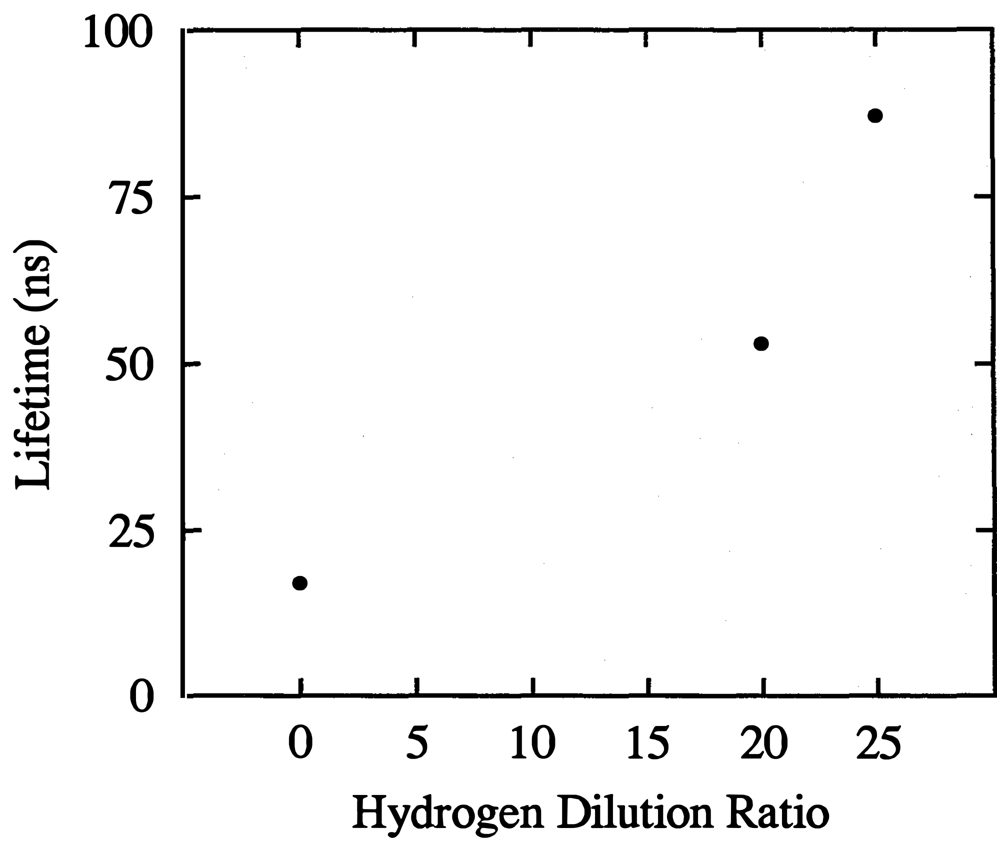


**Figure 10. Lifetime (at 480 K) of a-SiC:H films as a function of hydrogen dilution ratio.**

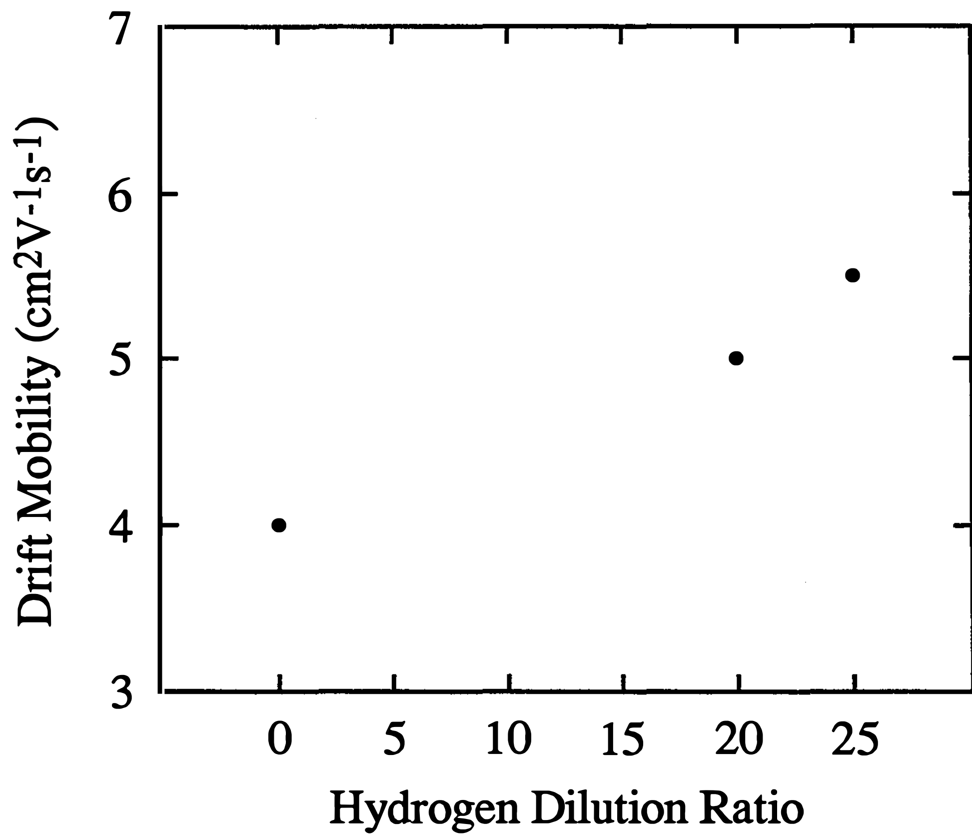


**Figure 11. Drift mobility (at 480 K) of a-SiC:H films as a function of hydrogen dilution ratio.**

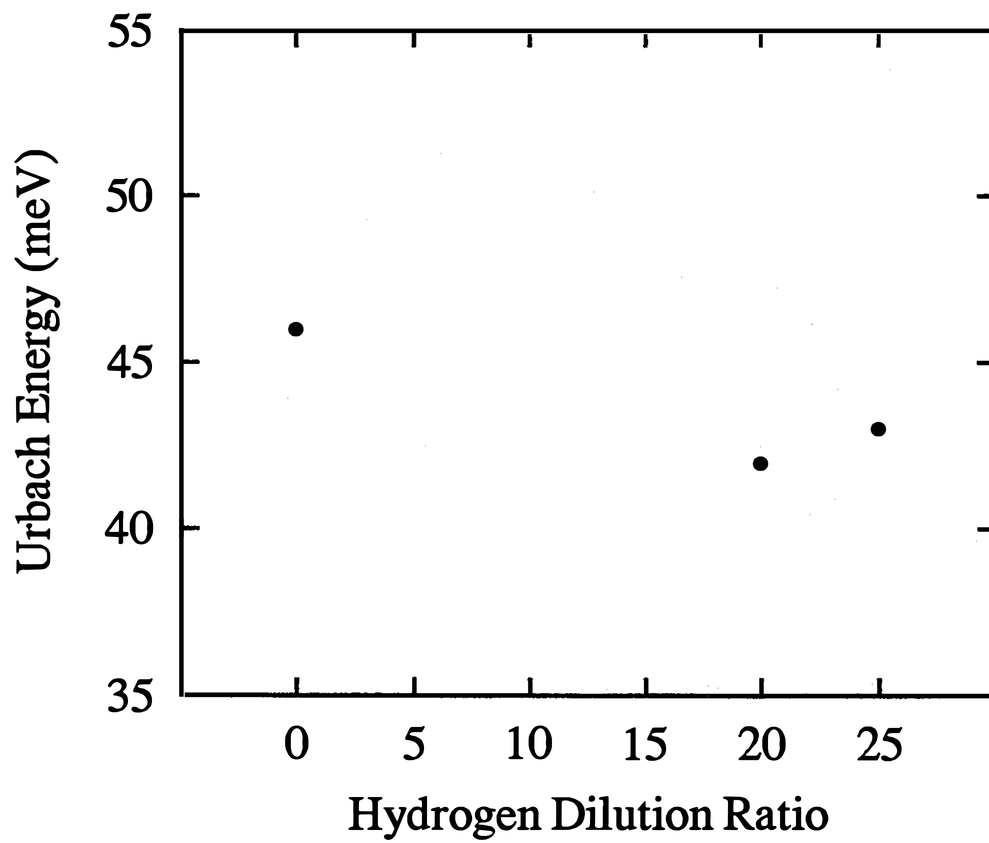


**Figure 12. Urbach energy of a-SiC:H films as a function of hydrogen dilution ratio.**

**Mobility and lifetime in annealed and light soaked conditions for glow discharge and hot wire intrinsic a-Si:H by photomixing**

We have utilized the capabilities of our photomixing technique to separately determine the mobility and lifetime under annealed and under light soaked conditions on samples prepared by various groups. Since it has been reported that higher stabilized cell efficiencies has been achieved utilizing i-layers grown under hydrogen dilution conditions our goal was to characterize such samples by our techniques and gain insight to the factors which determine the properties of these films.

Intrinsic a-Si:H films produced by the glow discharge (provided by NREL and Solarex) and the hot wire techniques (provided by NREL) were investigated with the photomixing technique. The sample characterizations are as follows.

**Table III.** Sample characterization

| Sample I. D. | Preparation | Provider | H Content | $T_s$ (C) | Thickness (nm) | Other |
|---|---|---|---|---|---|---|
| THD15 | Hot wire | NREL | 1% | 600 | 2200 | |
| THD16 | Hot wire | NREL | 11% | 350 | 2000 | |
| S#127i | Glow discharge | NREL | No H dil. | | 460 | |
| BK#1 | Glow discharge | NREL | 10% | | 590 | |
| D1203-2 | Glow discharge | Solarex | With H dil. | | 1200 | Light soaked for 600 h |
| D1203-3 | Glow discharge | Solarex | No H dil. | | 1500 | Light soaked for 600 h |

The mobility and lifetime were determined on the above samples under the conditions of *in situ* light soaking and under annealed conditions as a function of electric field and as a function of light intensity.

In situ light soaking measurements

In the in situ light soaking measurements, which were performed with a He-Ne laser with about 4 sun

intensities for 4 and 7 hours, mobility decays were found in various fashions. In general, the mobility decays for the hot wire samples (<20%) (Fig. 13) were found less than those of the glow discharge samples (~40%) (Fig. 14). This supports the findings that some hot wire samples are more stable than glow discharge samples under light soaking.

### Electric field dependence measurements of mobility

We employed our photomixing technique to measure the field dependence of the mobility and lifetime with the following results.

In the dc bias dependence measurements with the applied electric field ranging from 2000 V/cm to 9000 V/cm, the mobilities were found increasing and the lifetimes decreasing with increasing dc bias, while the $\mu\tau$ products remain essentially independent of the dc bias.

Four a-Si:H thin film samples provided by the National Renewable Energy Laboratory (NREL) were investigated by the photomixing technique. Samples THD15 and THD16 were produced by the hot wire process, with hydrogen contents about 1% and 11%, deposition temperatures of 600 C and 350 C, and thicknesses of 2200 nm and 2000 nm, respectively. Samples S#127i and B#1 were produced by the glow discharge process, with hydrogen content about 10% and thicknesses of 460 nm and 590 nm.

The electric field dependence of the drift mobility ($\mu_d$) and the lifetime ($\tau$) of these samples were measured both in the annealed state (4 hours at 180 C) and in the light soaked state (4 hours at 4 sun intensity). It was found that the drift mobility ($\mu_d$) increases with increasing electric field, while the lifetime ($\tau$) decreases with increasing electric field, and the $\mu\tau$ product is essentially independent of the electric field in the range from 2000 V/cm to 9000 V/cm. The fact that the lifetime decreases while the drift mobility increases indicates the existence of the diffusion limited transport and recombination[34] in all the samples in both the light soaked as well as the annealed states. It should be pointed out that in this case, the increase in $\mu_d$ with increasing field as well as the increasing in $\mu_d$ with increasing carrier density due to light illumination, which can possibly be explained by long-range potential fluctuations,[35-42] is compensated by the corresponding decrease in $\tau$, which can result in a field independent $\mu\tau$ or the commonly observed ohmic behavior of the photocurrent. In the presence of long range potential fluctuations, one would expect $\mu$ to increase with increasing electric field and with increasing carrier concentration.[43,46] Such increase in the drift mobility do not necessarily lead to an increase in the photoconductivity, since one commonly observes a corresponding decrease in $\tau$.

Fig. 15 and Fig. 19 show the electric field dependence of the drift mobility of these samples. The open dots and the solid dots are the experimental data in the annealed state and the light soaked state, respectively. The solid lines were obtained through a curve fitting procedure which will be discussed later. It is important to point out that the field dependence of the drift mobility is less in the light soaked state than that in the annealed state (Fig. 15 and Fig. 19).

Fig. 14 shows an empirical relationship between the field dependence of the drift mobility and the stability of the photoconductivity of the a-Si:H films under light soaking. The field dependence is characterized by

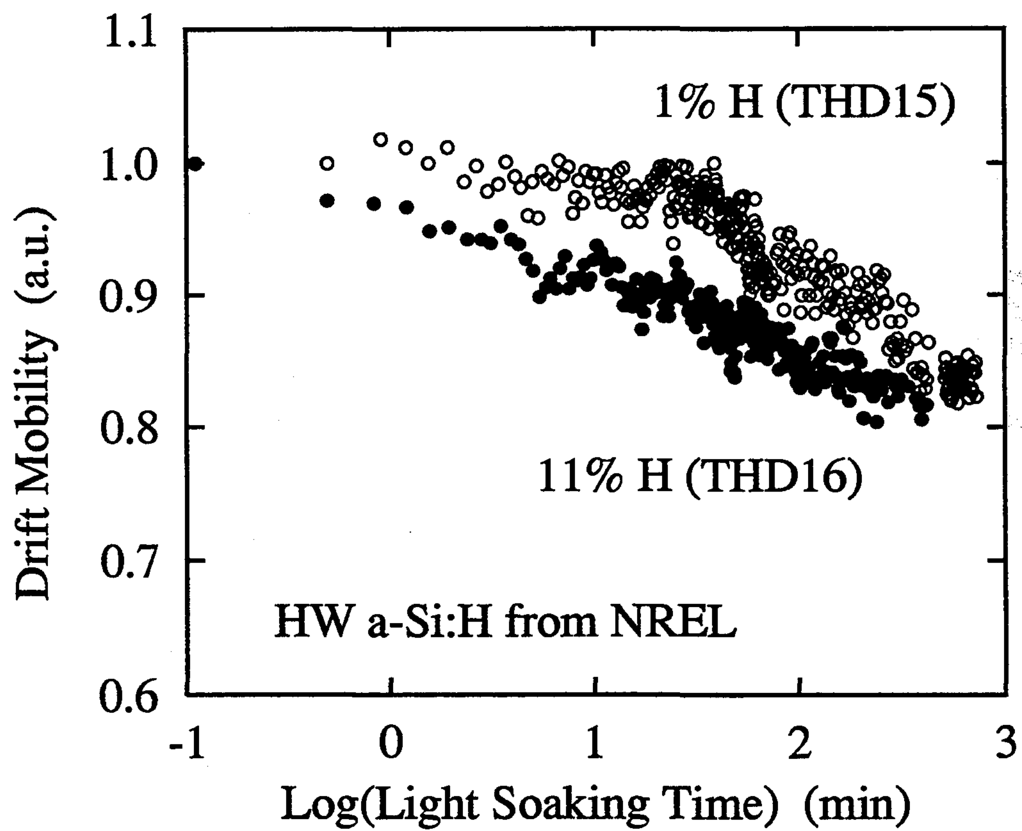


**Figure 13. Drift mobility versus light soaking time for the hot wire samples at 4 sun light intensity.**

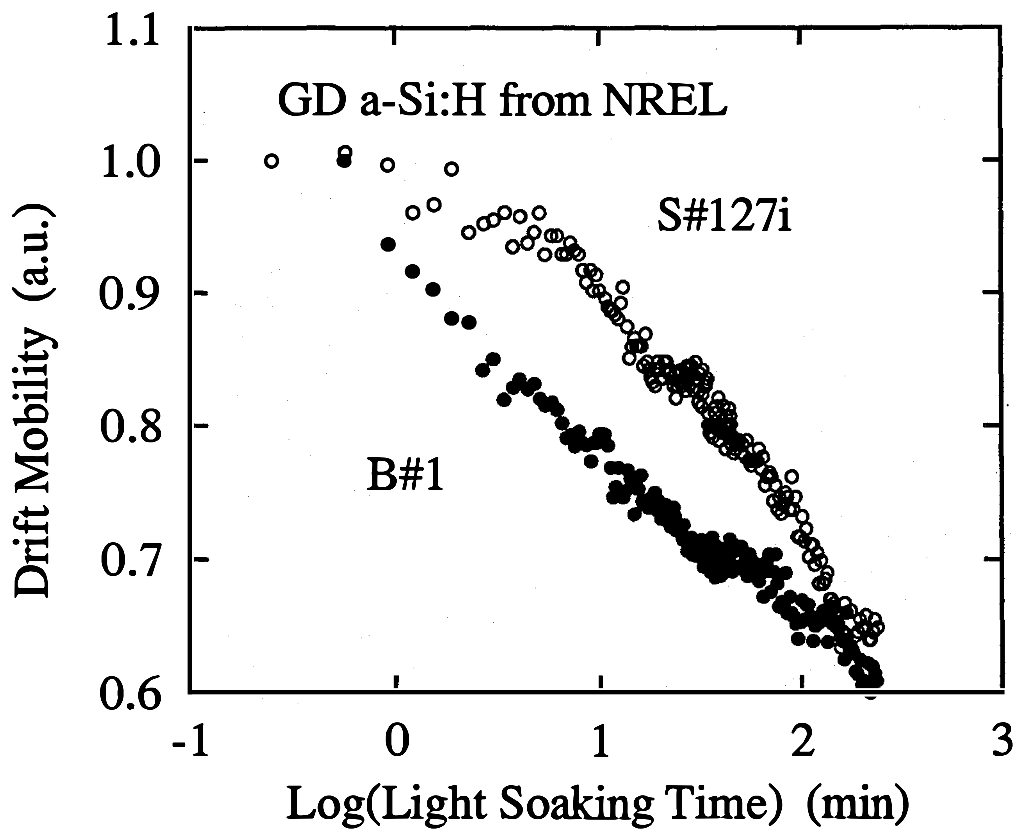


**Figure 14. Drift mobility versus light soaking time for the glow discharge samples at 4 sun light intensity.**

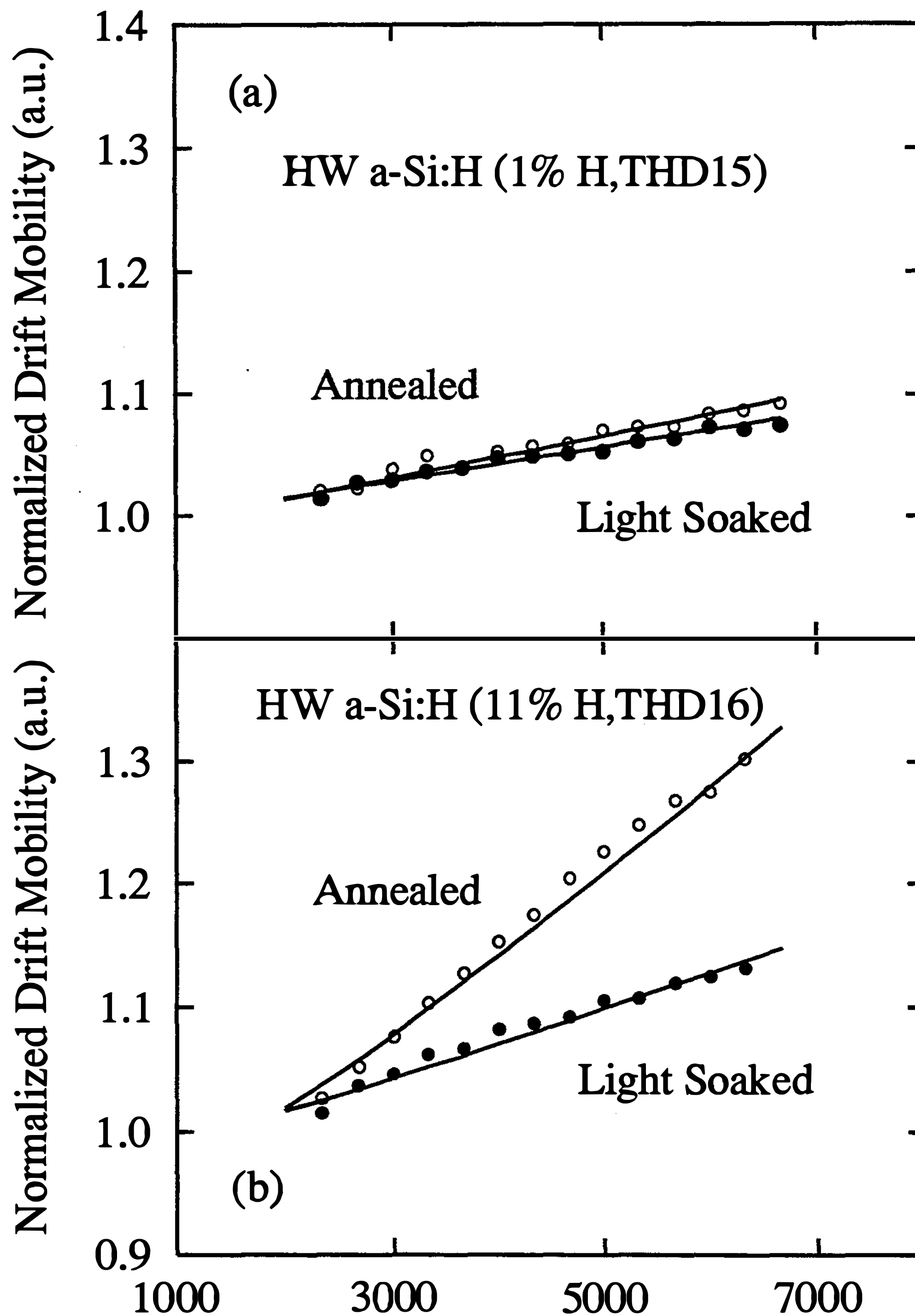


**Figure 15. Drift mobility versus applied electric field for the hot wire samples THD15 (1% H) (a) and THD16 (11% H) (b). Open and solid dots represent the data in the annealed and light soaked state respectively. Solid lines are curve fitting according to Eq. (25)**

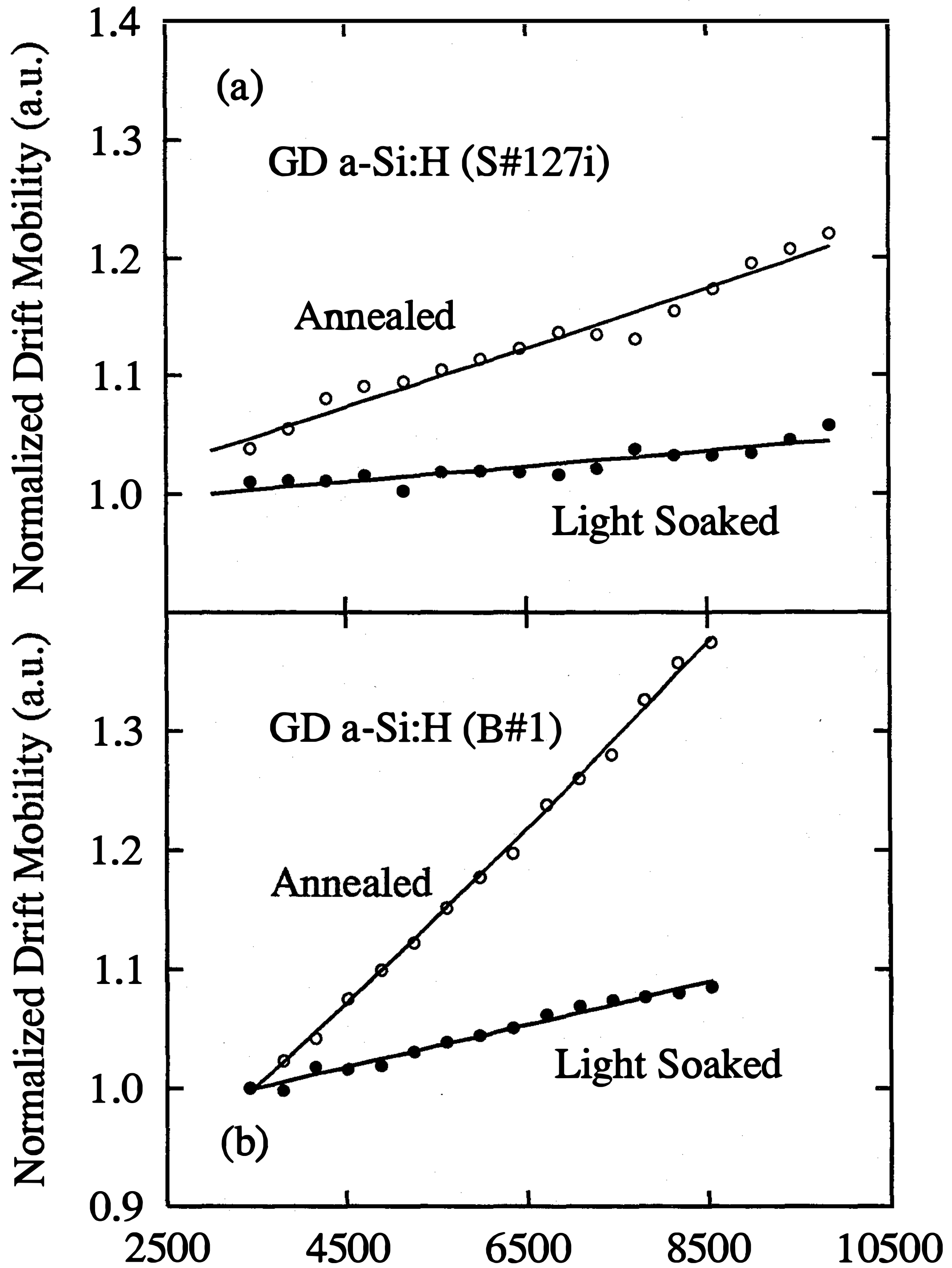


**Figure 16. Drift mobility versus applied electric field for the glow discharge samples S#127i (a) and B#1) (b). Open and solid dots represent the data in the annealed and light soaked state respectively. Solid lines are curve fitting according to Eq. (25)**

the average change in the normalized drift mobility to the change in the electric field, i.e., $\Delta\mu_d/\Delta E/\mu_d$, while the stability under light soaking is characterized by the ratio of the $\mu\tau$ product in the light soaked state (4 hours at 4 sun intensity) and to that in the annealed state (4 hours at 180 C), i.e., $(\mu\tau)_{LS}/(\mu\tau)_{AN}$. Consequently the smaller this ratio is, the less stable the sample is against light soaking.

It is clear from Fig. 16 that a greater field dependence of the drift mobility of an a-Si:H film in the annealed state indicates a poorer stability under light soaking, and vice versa. This empirical relationship is also supported by the experimental results that after light soaking the field dependence of the drift mobility of all a-Si:H films investigated decreases (Fig. 15 and Fig. 14). This empirical relationship indicates that the amount of light induced degradation is controlled by the generation of defects which are responsible for controlling the field dependence of the drift mobility in the annealed state. Important applications of this empirical relationship include the possibility of assessing the amount of expected light induced degradation without going through time consuming light soaking experiments and possible *in situ* evaluation of stability, e.g., during sample preparation processes to find the optimal conditions for stable samples. The results to be discussed later and was also reported in the literatures.[43]in Fig. 16 agree with our observation that light soaking decreases the magnitude of $\mu_d$.The light induced defects as well as the native defects, which serve as recombination centers and trapping centers, can be charged and can form certain potential barriers or fluctuations. In the transport process, the charged carriers can either go over the potential barrier through thermal activation or go around the potential barrier through scattering. If the former dominates the latter, then through simple statistical calculations one can obtain the following electric field (E) dependence of the drift mobility $\mu_d(E)$:[44]

$$\mu_d(E) = \mu_d^0 \exp\left(-\frac{eV_P}{kT}\right)\frac{eLE}{kT\left[1-\exp\left(-\frac{eLE}{kT}\right)\right]} \qquad (if\ |LE| \le V_P)$$

$$\mu_d(E) = \mu_d^0 \frac{\exp\left(-\frac{eV_P}{kT}\right)}{\frac{kT}{eLE}+\left(1-\frac{V_P}{LE}-\frac{kT}{eLE}\right)\exp\left(-\frac{eV_P}{kT}\right)} \qquad (if\ |LE| > V_P) \tag{25}$$

where $\mu_d^0$ is the drift mobility without the potential fluctuations, while Vp and L are an average magnitude and range of the potential fluctuations, respectively.

The range L of the potential fluctuations can be determined through curve fitting using the above equation to the experimental data shown in Fig. 15 and Fig. 14 (Table IV, "Experimental and curve fitting results for electric field dependence of mobility.," on page 39). The range of the potential fluctuations in the light soaked state ($L_{LS}$) was found up to a factor of 4 smaller than that in the annealed state ($L_{AN}$) (Table I). An increase in the internal electric field leads to increased electronic inhomogeneity in the samples. It has been previously suggested that such an increase in the inhomogeneity may lead to stabilization of the degradation process.[45]

Our model is similar, but not limited, to the model of long-range potential fluctuations, which has been conjectured to have significant influences on the transport properties. During the light soaking process, the

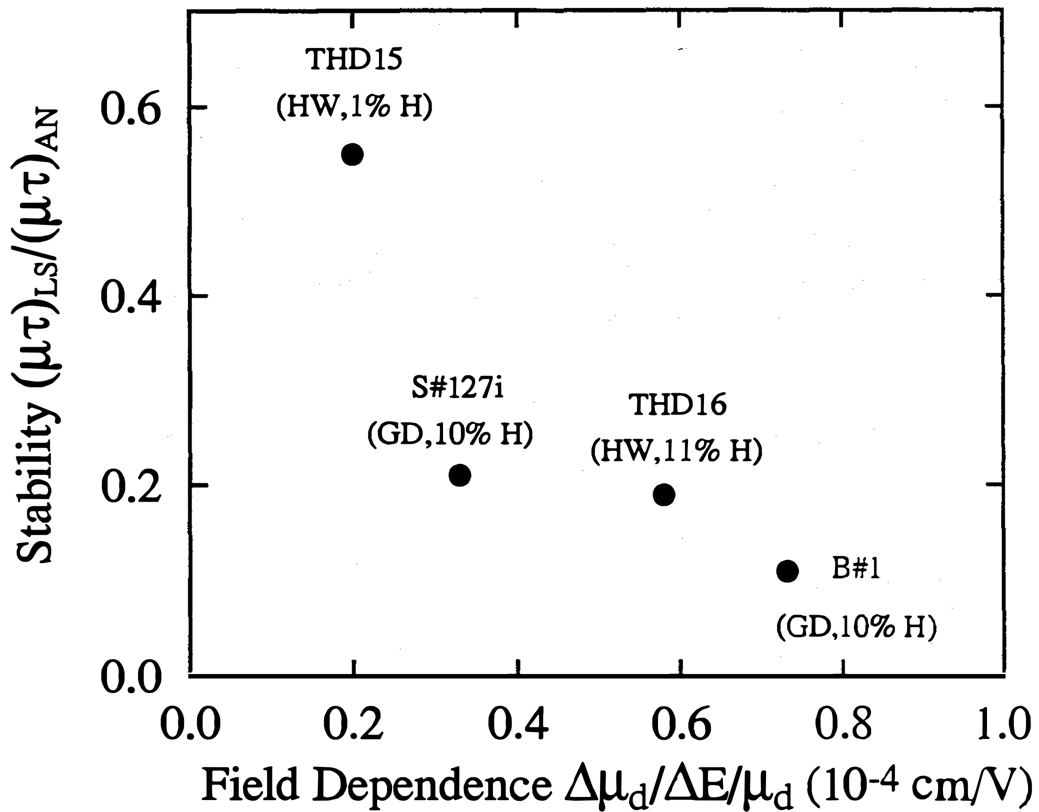


**Figure 17. Electric field dependence of of drift mobility ($\Delta\mu_d/\Delta E/\mu_d$) versus stability (is characterized by the average change in the normalized drift mobility to the change in the electric field, i.e., Dmd/DE/md, while the stability $(\mu\tau)_{LS}/(\mu\tau)_{AN}$) Of the a-Si:H films under light soaking.**

magnitude ($V_P$) of the potential fluctuations has a tendency to increase, whereas the range (L) of the potential fluctuations has a tendency to decrease. But because of the long range nature of the potential fluctuations, the potential fluctuations should be spatially nondegenerate. Therefore, during the light soaking process, the magnitude ($V_P$) of the potential fluctuations should not increase as significantly as the range (L) of the potential fluctuations decreases. This is partially evidenced by the experimental results that the field dependence of the drift mobility is less in the light soaked state than that in the annealed state (Fig. 15 and Fig. 14).

It is reasonable to assume that the charged defects are responsible for the long-range potential fluctuations. In a-Si:H, a reasonable candidate for the charged defects is the charged dangling band state ($T_3^{+/-}$). Just as in the case of neutral dandling bonds ($T_3^0$), a fraction of the charged dangling bonds ($T_3^{+/-}$) is stable, while another fraction in metastable, i.e., the density of the latter increases upon light soaking and decreases upon annealing. The existence of the stable and metastable charged dangling bonds ($T_3^{+/-}$) has been attributed to the local dipole potential fluctuations.[38] In the context of this letter, it is not important to differentiate whether a $T_3^{+/-}$ defect is newly created or it is converted from a $T_3^0$ defect. Assuming that the density (n) of the $T_3^{+/-}$ defects is determined by:[40,41]

$$n \propto V_P^2/L, \tag{26}$$

we can estimate the lower limit of the ratio of the defect densities in the light soaked state ($n_{LS}$) and that in the annealed state ($n_{AN}$) can be estimated by $n_{LS}/n_{AN} = L_{AN}/L_{LS}$, where $L_{AN}$ and $L_{LS}$ (Table I) are the ranges of the potential fluctuations in the annealed and light soaked states, respectively. The results of such ratios are also included in Table IV.

**Table IV.** Experimental and curve fitting results for electric field dependence of mobility.

| Sample ID | Preparation | H Content | $(\mu\tau)_{AN}/(\mu\tau)_{LS}$ | $L_{AN}$ (Å) | $L_{LS}$ (Å) | $n_{LS}/n_{AN}$ |
|---|---|---|---|---|---|---|
| THD15 | Hot Wire | ~1% | 1.8 | 82 | 64 | 1.3 |
| THD16 | Hot Wire | ~11% | 5.3 | 345 | 133 | 2.6 |
| S#127i | Glow Discharge | ~10% | 4.8 | 128 | 33 | 3.9 |
| B#1 | Glow Discharge | ~10% | 9.1 | 383 | 92 | 4.2 |

In conclusion, by using the photomixing technique we have found that the drift mobility ($\mu_d$) of intrinsic hydrogenated amorphous silicon (a-Si:H) films produced by both glow discharge and hot wire techniques increases with increasing electric field, and a greater field dependence of the drift mobility of an a-Si:H film in the annealed state indicates a poorer stability under light soaking, and vice versa. This empirical relationship indicates that the amount of light induced degradation may be predictable from the field dependence of the drift mobility in the annealed state. The results can be analyzed employing the model of the long-range potential fluctuations, as the lower limit of the density of defects (normalized to that in the

annealed state) after light soaking determined by this model ($n_{LS}/n_{AN}$) is about 40% to 80% of the total density of defects (normalized to that in the annealed state) responsible for SWE which can be estimated by $(\mu\tau)_{AN}/(\mu\tau)_{LS}$ (Table I). It should be pointed out that our results suggest that the light induced charged dangling bonds may not affect $\mu\tau$ by increased recombination, but rather by affecting $\mu_d$ through controlling potential fluctuations in the sample. It has been found that upon light soaking both $\tau$ and $\mu_d$ decease following different stretched exponential laws.[4] Stretched exponential behavior is typical for hierachically constrained systems, and transport phenomena appear to provide a barrier or constraint for degradation phenomena.[47]

### Electric field dependence of mobility of compensated a-Si:H samples

We have previously determined the drift mobility and recombination lifetime in a series of compensated a-Si:H by photomixing that had been measured earlier by the time-of-flight technique by the Xerox group. We had found that the drift mobilities decreased as the compensation increases and could be accounted for by existence of long-range potential fluctuations. To further extend our understanding of the electric field dependence of the drift mobility as influenced by long-range potential fluctuation, we performed the photomixing measurements as a function of electric field on several compensated samples in the field regime from 2000 V/cm to 10000 V/cm. These compensated a-Si:H samples were provided by Dr. R. A. Street of Xerox and were made by plasma deposition of SiH with equal volume concentrations of $B_2H_6$ and $PH_3$. The samples employed had the following concentration ratios of $B_2H_6$ and $PH_3$ to $SiH_4$ in the deposition gas: $10^{-4}$ and $10^{-3}$, which will be referred to as the compensation concentration. In order to measuring the quite low mixing signal of compensated samples, a lock-in amplifier was used.

Fig. 18 and Fig. 19 show the electric field dependence of the drift mobility for compensation $10^{-4}$ and $10^{-3}$ respectively. The open dots are the experimental points while the solid lines were obtained through a curve fitting procedure of a statistical model for the electric field dependence of mobility which we will describe later on. The ranges of the potential fluctuations derived from curve fitting are 570 Å and 360 Å for the samples with compensation concentration $10^{-4}$ and $10^{-3}$ respectively. This results can be explained that raising the doping concentrations will reduce the range and increase the magnitude of the potential fluctuations.

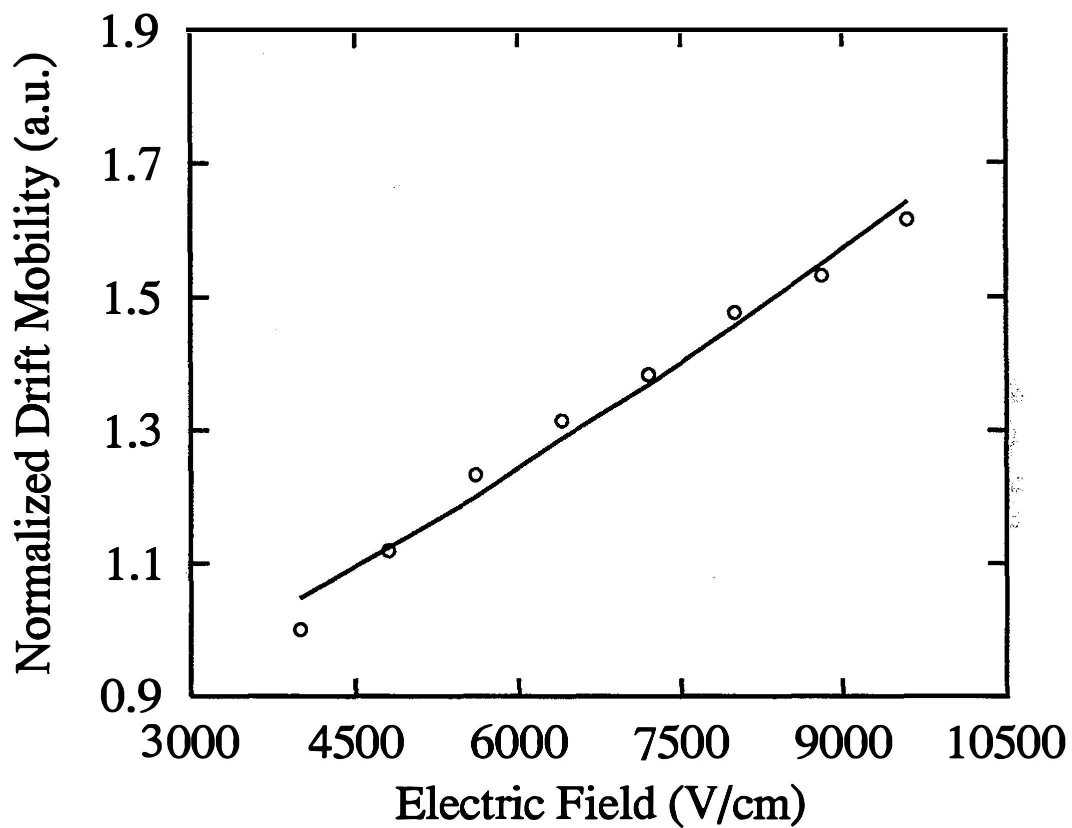


**Figure 18. Drift mobility of compensated a-Si:H film with compensation level of $10^{-4}$ versus electric field.**

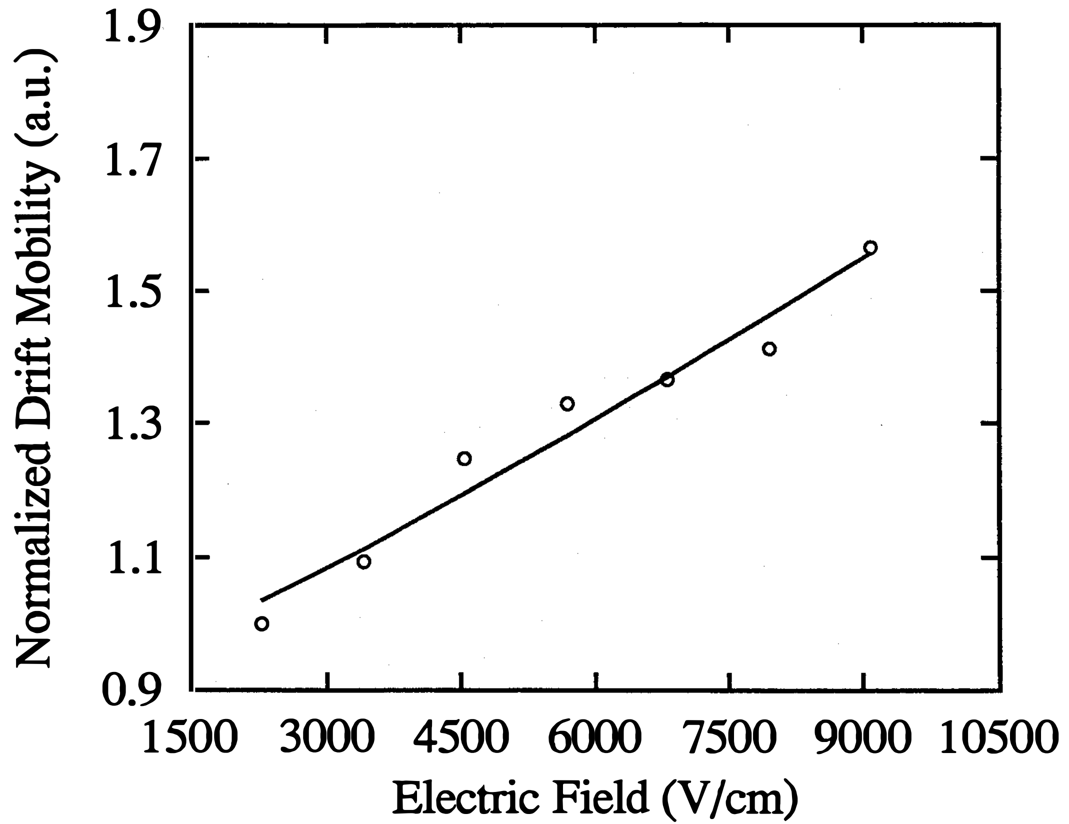


**Figure 19. Drift mobility of compensated a-Si:H film with compensation level of $10^{-3}$ versus electric field.**

## Light intensity dependence measurements

In the light intensity dependence measurements, the lifetimes were found decreasing with increasing light intensity, while the mobilities were found increasing with increasing light intensity (Fig. 14 through Fig. 14) except for the mobilities of the hot wire samples in the light soaked state which show a peak at an intermediate light intensity (Fig. 14 and Fig. 14).

The decrease of lifetime with increasing light intensity is commonly attributed to the increased splitting of the quasi fermi levels and thus increased number of recombination centers.

The change of mobility with increasing light intensity essentially is the result of competition between the enhanced screening effects which reduce the long range potential fluctuations and the increased change occupation in the localized states due to increased quasi fermi level splitting which enhances the long range potential fluctuations.

The peak in the mobility versus light intensity curve for the hot wire samples in the light soaked state indicate that the (charged) defects generated by the light soaking processes are swept through by the quasi fermi levels when the light intensity changes.

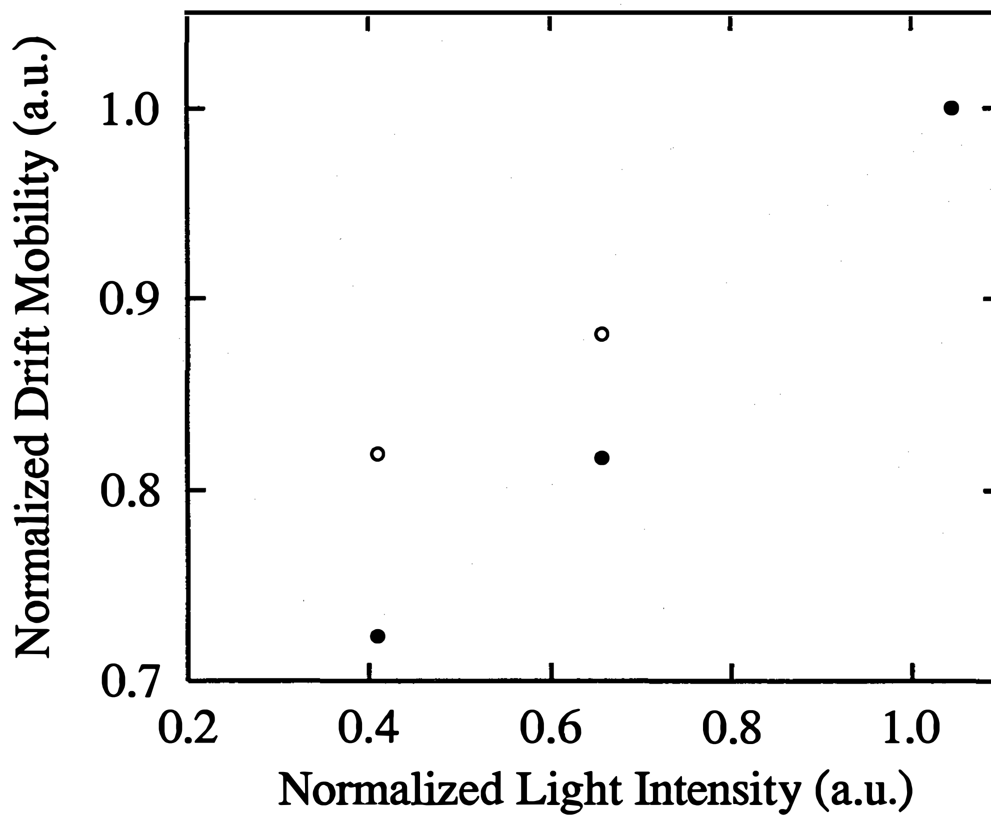


**Figure 20. Drift mobility versus light intensity for the glow discharge sample BK#1. Open and solid circles represent the annealed and light soaked (4 sun, 4 hours) state respectively.**

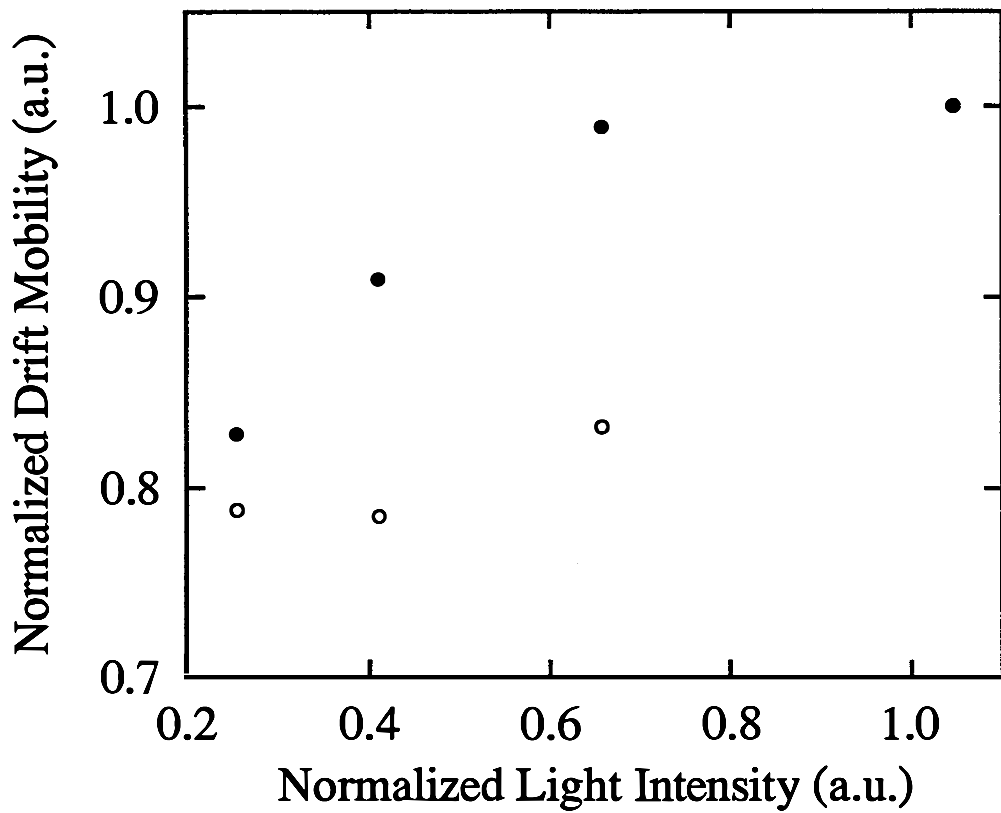


**Figure 21. Drift mobility versus light intensity for the hot wire sample THD16. Open and solid circles represent the annealed and light soaked (4 sun, 7 hours) state respectively.**

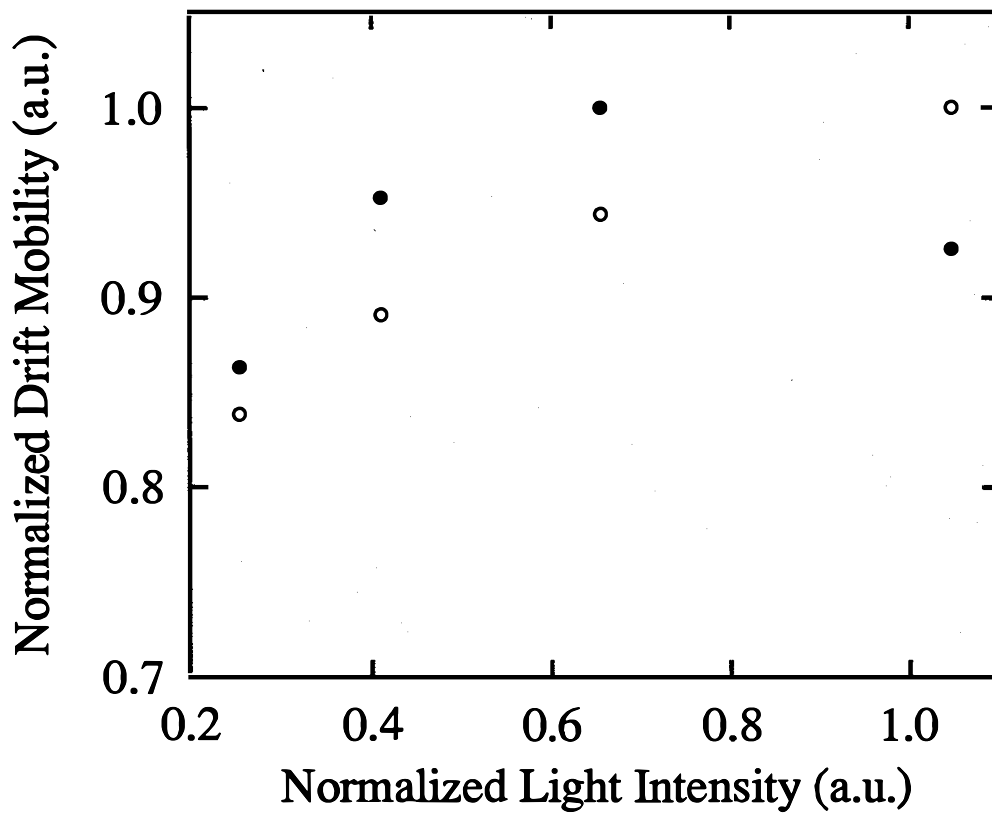


**Figure 22. Drift mobility versus light intensity for the hot wire sample THD15. Open and solid circles represent the annealed and light soaked (4 sun, 7 hours) sate respectively.**

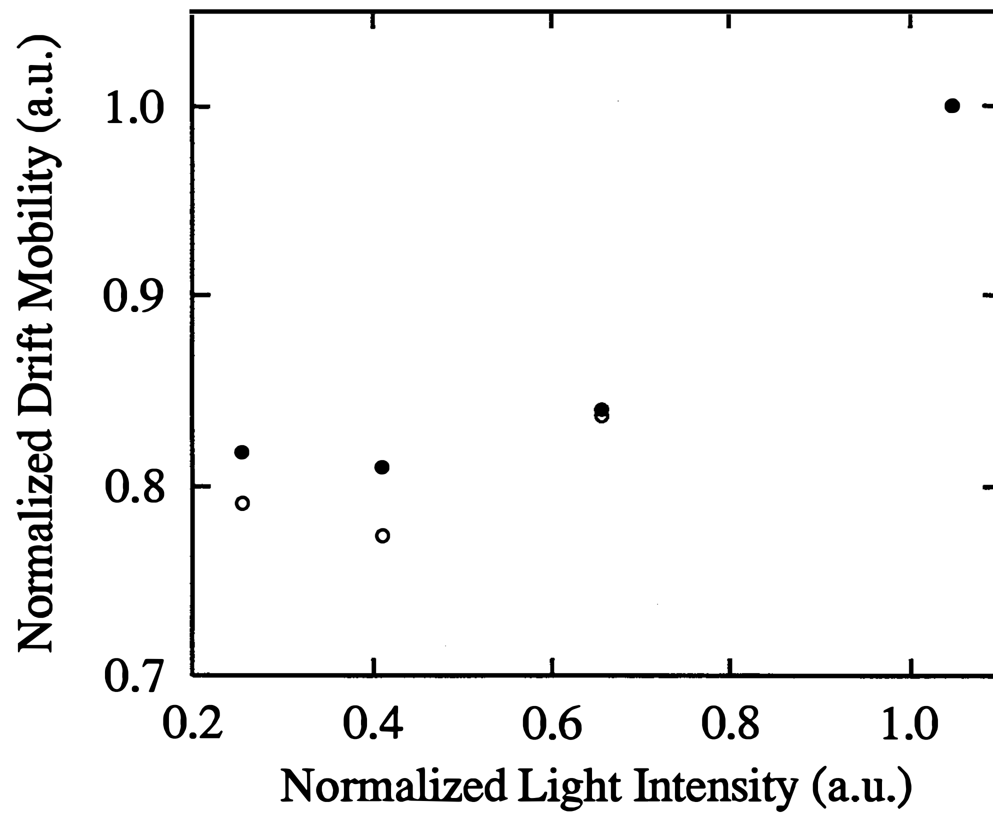


**Figure 23. Drift mobility versus light intensity for the Solarex samples. Open and solid circles represent sample D1203-2 and sample D1203-3 respectively in the light soaked (1 sun, 600 hours) state.**

## Photoelectron emmission 1n air from amorphous semiconductors and transparent conducting oxides

It is well established that photoelectron spectroscopy is a method to determine near surfaces electronic properties of amorphous semiconductors and detecting chemical impurities on surfaces; however the technique usually requires an ultrahigh-vacuum environment and is not readily adaptable to analytic procedures which can ultimately be used on the production line.

If photoemission measurements could be performed in air, it would prove to be a useful technique that would be readily adaptable for the detection of surface contaminants and monitor cleanliness in the production environment; in addition, if the photoemission yield could be scanned over small as well as large areas and non-uniformities detected, micro-shunting problems in solar cells could be identified.

We have available in our laboratory an apparatus that can perform optically stimulated electron emission from semiconductors surfaces in air. The principle of the technique consists of the following:

When metal or semiconductor surfaces are illuminated with ultraviolet light with the proper wavelength, electrons are emitted from the surface. The emitted and subsequently scattered electrons can be collected across an air gap. By maintaining the surface collector distance relatively constant, changes in the measured photocurrent (which is of the order of $10^{-10}$ to $10^{-12}$ A) can provide information about the surface, e.g., electronic structure and chemical composition. Any contaminant on the surface, depending on its photoemission, can either enhance or attenuate the inherent emission from a clean surface. In addition, the probe can be scanned over the surface and thus provide a two dimensional display of the surface characteristic. The excitation source consists of a Hg lamp with the 5eV and the 6.7eV lines which are adequate for photoemission from metals and semiconductors of interest for photovoltaic cell production.

We have performed photoemission measurements on a-Si:H films produced at NREL. Figure 24 shows the results for a 4 inch by 4 inch sample indicating the non-uniformity due to possible inhomogeneity of composition and the positioning of the sample substrate in the glow discharge.

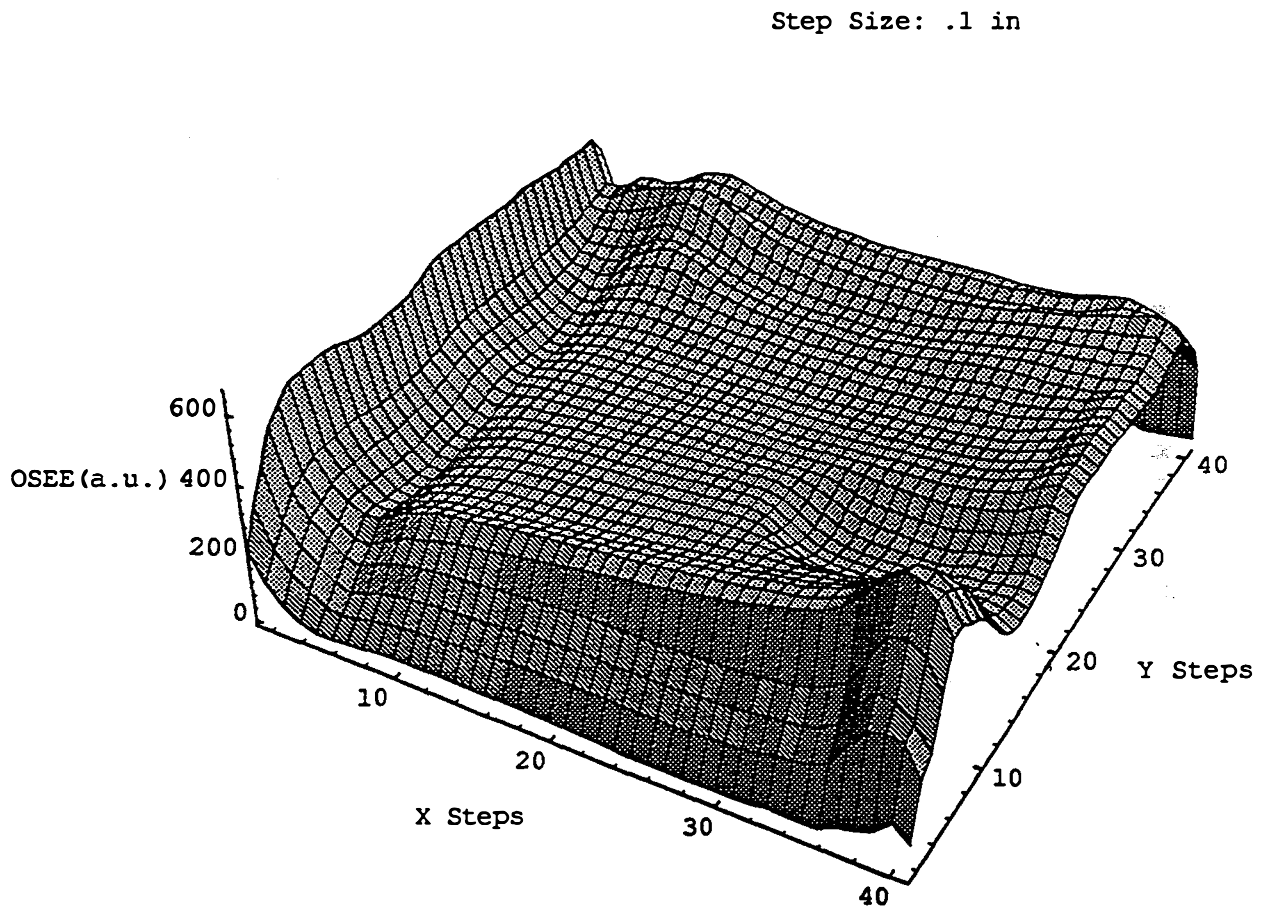


**Figure 24. Inhomogeneity of NREL a-Si:H film detected by the Optical Stimulated Electron Emission (OSEE) technique.**

We obtained a series of transparent conducting oxide (TCO) films from S. Hegedus of Iowa State University to perform Optically Stimulated Electron Emission (OSEE) measurements. They are consisted of TCO films of $SnO_2$ and ZnO both textured and untextured and films of a-SiC:H on ZnO. Some of the TCO films were virgin and others were exposed to index matching organic liquids for optical measurements and then subsequently subjected to degreasing and cleaning with TCE and Freon. This apparatus enables us to profile the barrier height on a surface up to 4 inches by 4 inches in area in air; thus it can be employed under normal production environment conditions to monitor possible in-process surface changes of barrier heights. In our previous report we presented results on a-Si:H films produced by NREL which revealed some non-uniformity of barrier height due possibly to inhomogeneity of composition, due perhaps to the positioning of the sample substrate in the glow discharge. We also referred to some results on TCO samples supplied by Steven Hegedus. We will now present more detailed data on the TCO samples as well as photoemission from a range of substances that maybe of general interest to other teams.

The TCO samples described by S. Hegedus are as follows: The TCO surfaces were cleaned with TCE, freon, and DI water before sending them to us since on index matching liquid was applied to perform optical measurements on the textured surfaces. In addition a few identical pieces that had not been exposed to the index matching liquid were run to compare the effect of the degreasing and cleaning in the TCE and freon. All textured TCO layers were 0.8-1.0 μm thick. The TCE 4375 and 4376 series were exposed to an organic fluid and then cleaned in TCE and freon. The following is the description of the samples:

| Number | Sample description |
|---|---|
| 4375-11 | text. SnO2 from Solarex (standard device substrate) |
| 4375-12 | text. ZnO from Solarex |
| 4375-21 | text. ZnO from Utility PV Group (UPG) |
| 4375-22 | text. ZnO from Harvard (Prof. Gordon's Group) |
| 4376-11 | 200 Å a-SiC p-layer deposited at IEC on 4375-11 |
| 4375-12 | 200 Å a-SiC p-layer deposited at IEC on 4375-12 |
| 4376-21 | 200 Å a-SiC p-layer deposited at IEC on4375-21 |
| 4376-22 | 200 Å a-SiC p-layer deposited at IEC on4375-22 |
| | |
| A | virgin sample of 4375-11 |
| B | virgin sample of 4375-12 |
| C | virgin sample of 4375-21 |
| | |
| 91539-21 | 1000 Å specular ZnO (no texture) sputtered at IEC |
| 91552-17 | 200 Å specular ZnO sputtered on text. SnO2 |
| 91554-04 | 1000 Å specular ZnO sputtered on text. SnO2 |
| E | 1000 Å specular $SnO_2$ grown on text. ZnO (Harvard) |

Results:

The following figures are the results of the photoemission from the various combinations of samples described in the above table. The photoemission in air was obtained using a Hg lamp as the illuminating source and collecting the electrons across a narrow air gap. The light source and the collector were scanned over the surface of the sample using stepping motors. The x-steps and y-steps were at intervals of 0.05 inches and the optically stimulated electron emission (OSEE) in arbitrary units is displayed on the z-axis. The photocurrents were of the order of $10^{-11}$ to $10^{-12}$ amps and provide information about the barrier

heights or any contaminants on the surface. Any containments on the surface can either enhance or attenuate the inherent emission from a clean surface.

Figure 25 through 32 show the results for samples 4376-11, 4376-21, 4376-12 and 4376-22 respectively. These were 200A a-SiC p-layers deposited by IEC on textures substrates 4375-11, 4375-21, 4375-12, and 4375-22 respectively. The sources of the substrates are shown in the above. These figures show a spatial variation in the electron yield which may be due to the surface or the interface between the TCO and the a-SiC layers. The dominant Hg lines responsible for the photoemission are the 5 eV and the 6.7 eV lines. The optical measurements on these samples have been recently supplied by Steven Hegedus which will allow us to ascertain surface or volume penetration.

Figure 29 shows the yield from sample 4375-11, the textured $SnO_2$ film, which was coated with an organic index matching layer for optical measurement and then was cleaned with TCO, freon and DI water as compared to sample A which is a virgin sample of 4375-11, the textured $SnO_2$ film from Solarex. It is clear that the cleaning procedure leaves no residue.

Figure 30 is a comparison of samples 4375-12, 4375-22 and sample B. From the yeild of the samples, it is clear the cleaning procedures leaves no residue.

Figure 31 compares samples 91539-21, 91552-17, 9153-04 and sample E which are 1000 Å specular ZnO (no texture) sputtered at IEC, 200 Å specular ZnO sputtered on textured $SnO_2$ , 1000 Å specular ZnO sputtered on textured $SnO_2$ and 1000 Å specular $SnO_2$ grown on textured ZnO from Harvard. The barrier heights are relatively the same on all these samples.

Finally Figure 32 compares sample A the virgin sample of 4375-11, the textured SnO2 from Solarex with sample C the virgin sample of 4375-21, the textured ZnO sample from Utility PV Group (UPG). It should be noted that for sample 4375-21 two regions of stripped increased yield were observed. Visual examination indicates a yellow discoloring in this region relative to the rest of the film. Hegedus has indicated that he would be interested in obtaining the absolute values of the barrier heights of the TCO films after various treatments; we are looking into this matter.

It should be noted that for all the TCO samples have less yields than the p-layers of a-SiC:H deposited on the TCO films. This is probably due to that the a-SiC:H films have lower bandgaps than the TCO films. The optical data supplied by S. Hegedus is being analyzed to answer this question.

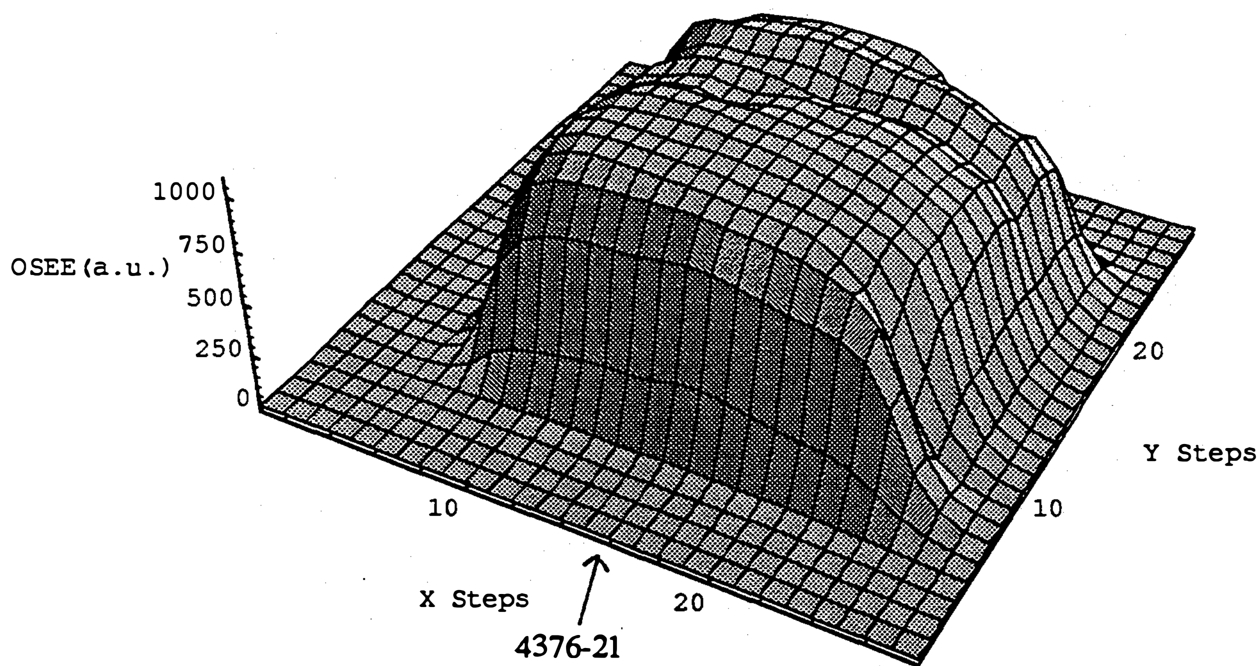


**Figure 25. Photoemission in air from sample 4376-21: 200 Å of a-SiC p-layer deposited at IEC on layer 4375-22, texture ZnO from Harvard (Prof.Gordon's Group).**

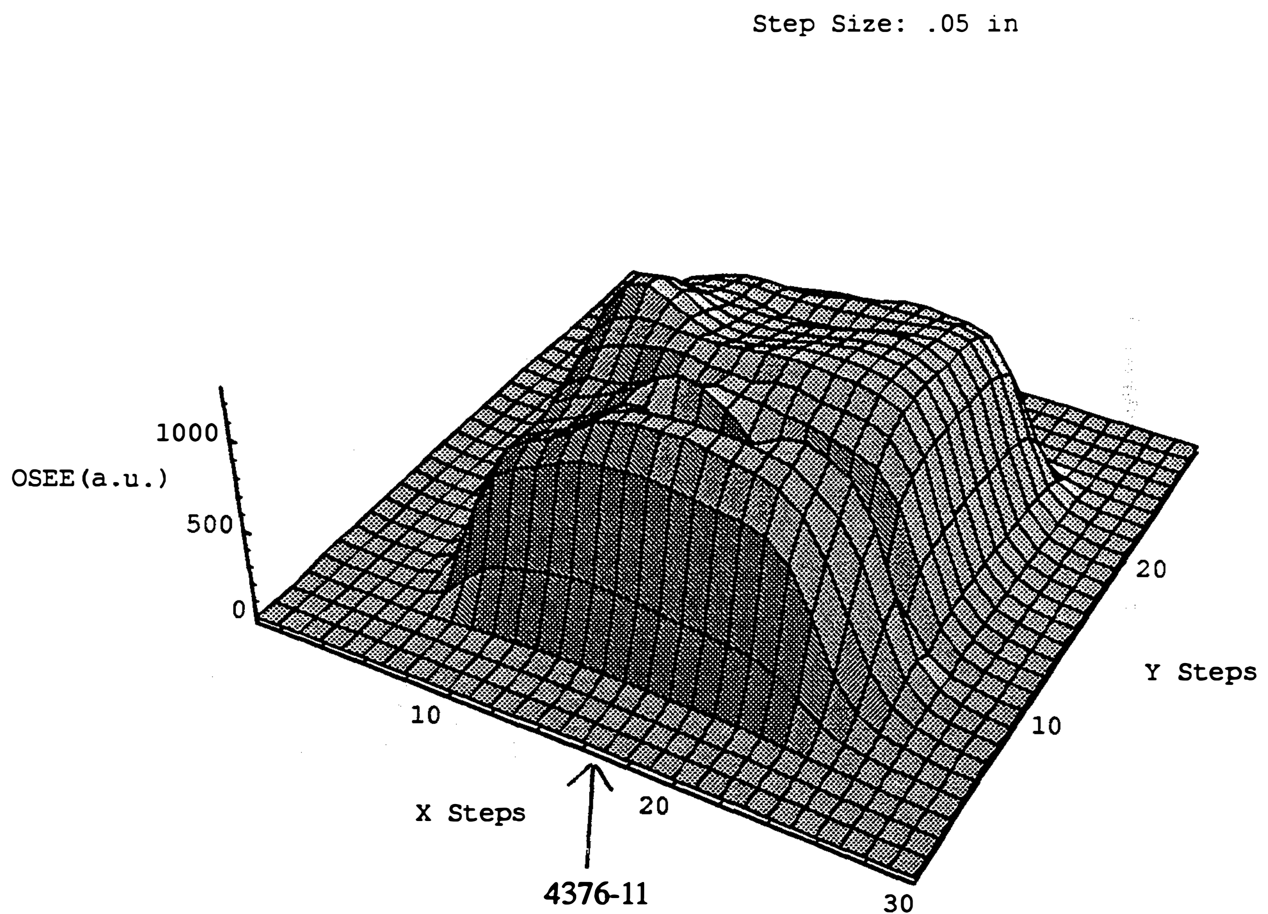


**Figure 26. Photoemission in air from sample 4376-11: 200 Å of a-SiC p-layer deposited at IEC on sample 4375-11, textured $SnO_2$ from Solarex (standard device substrate).**

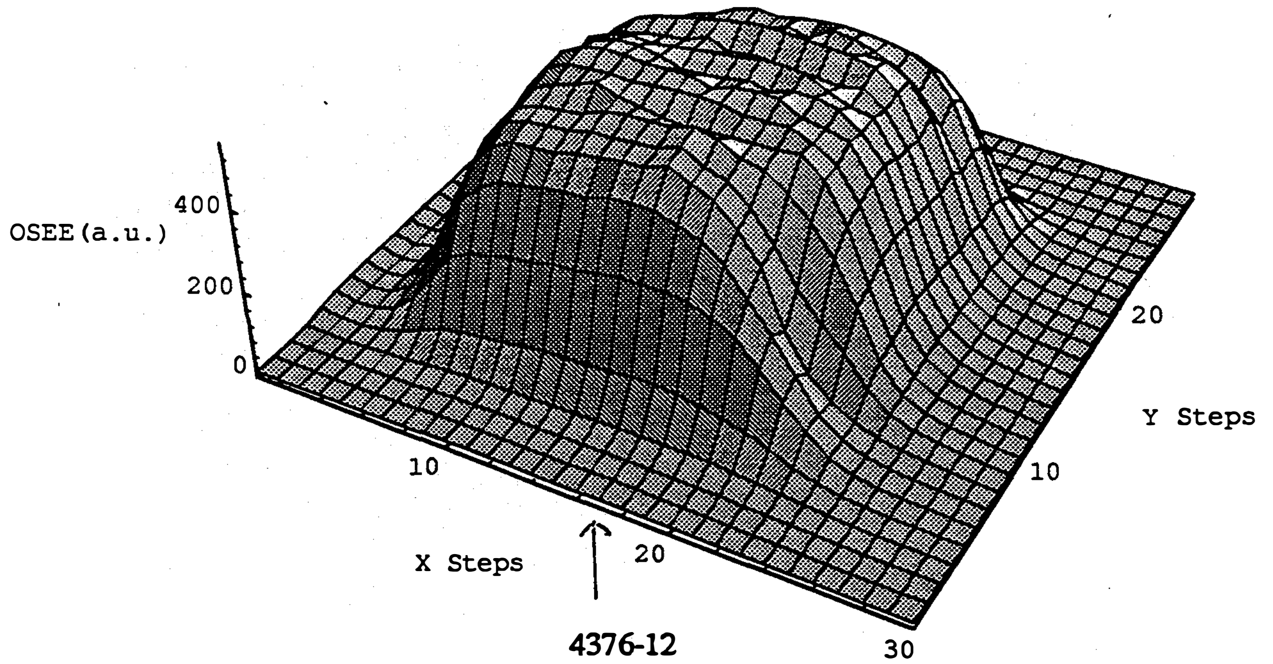


**Figure 27. Photoemission in air from sample 4376-12: 200 Å a-SiC p-layer deposited at IEC on layer 4375-12, textured ZnO from Solarex.**

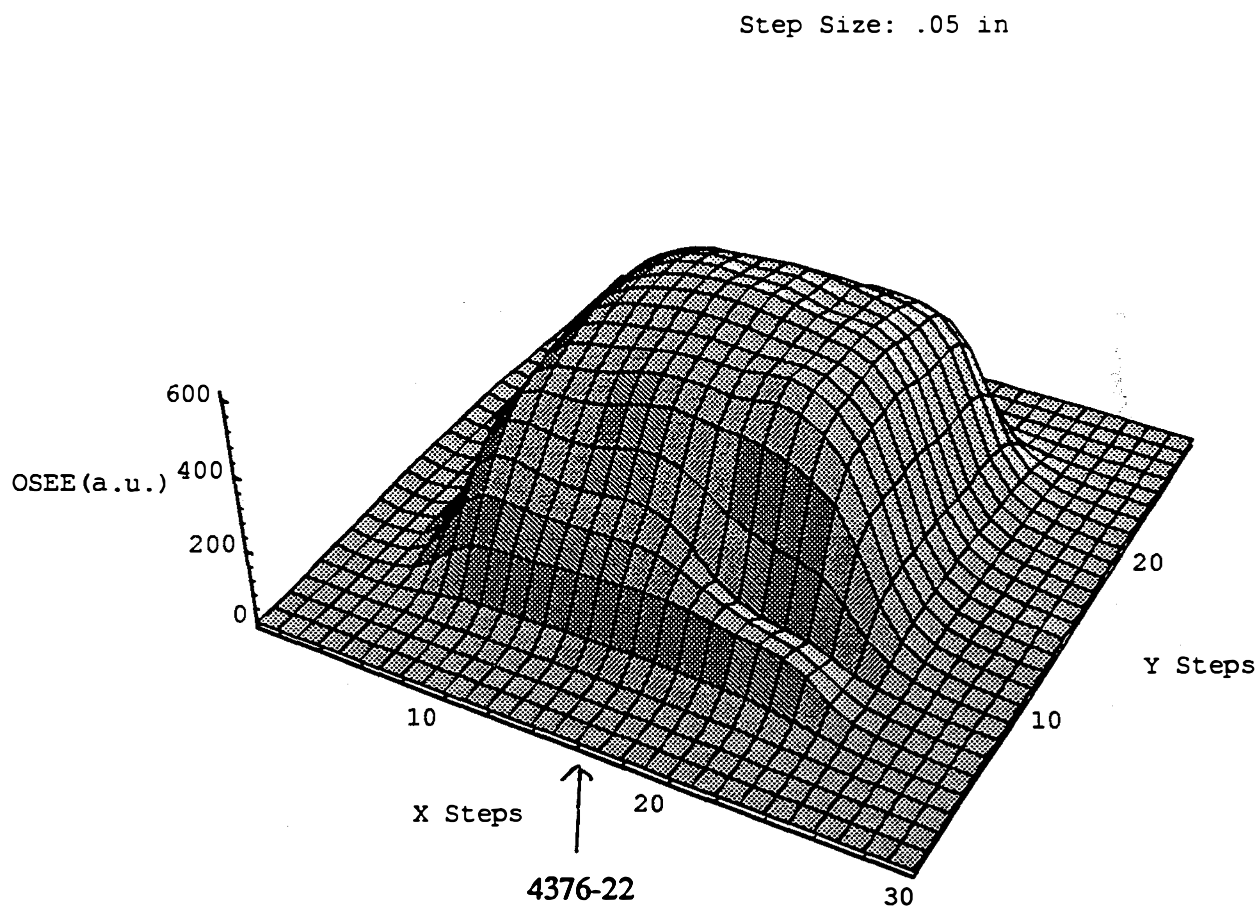


**Figure 28. Photoemission in air from sample 4376-22: 200 Å a-SiC p-layer deposited at IEC on 4375-22, textured layer ZnO from Harvard (Prof. Gordon's Group).**

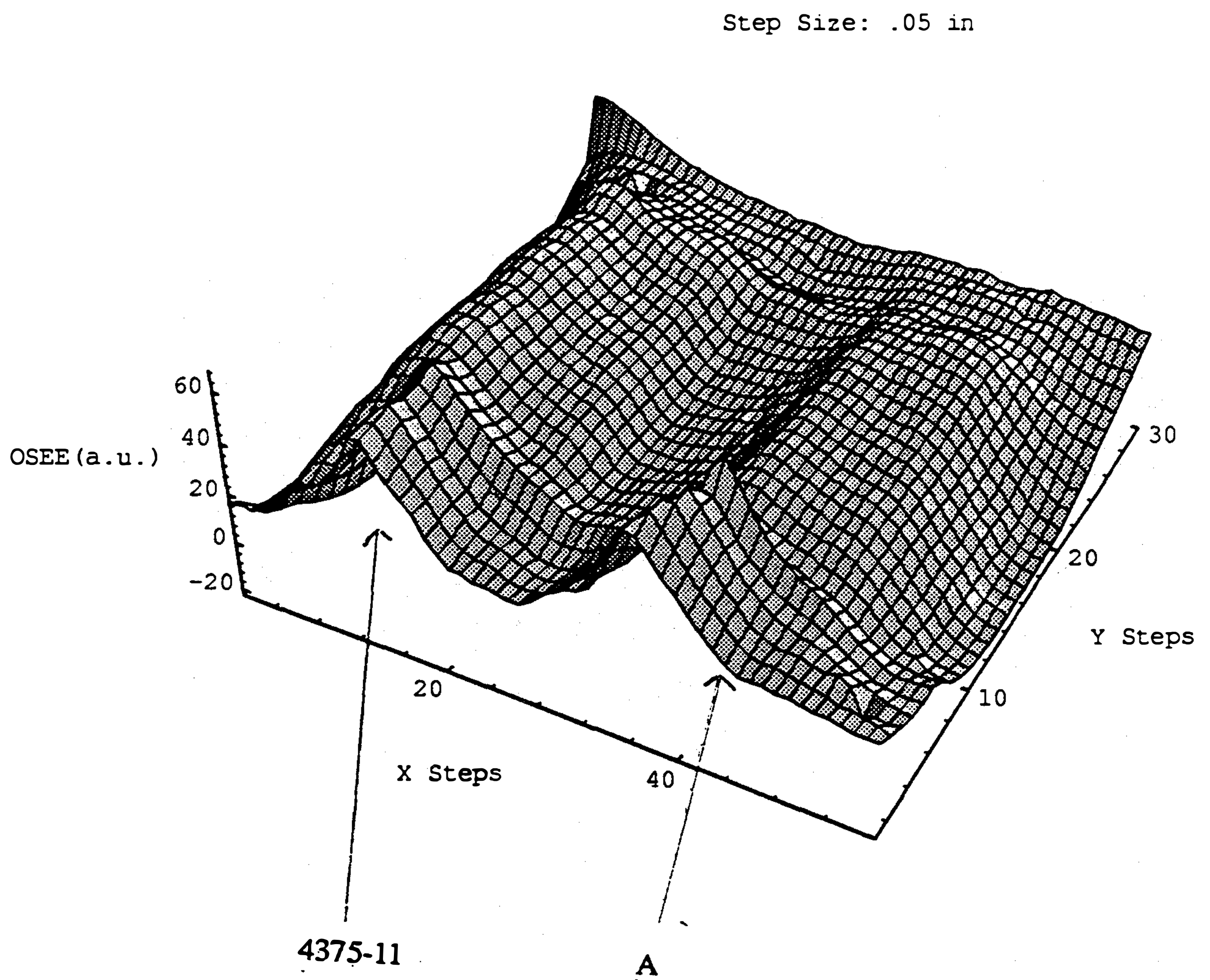


**Figure 29. Comparison of the photoemission in air between samples: 4375-11: textured $SnO_2$ from Solarex (standard device substrate) and A: virgin sample of 4375-11.**

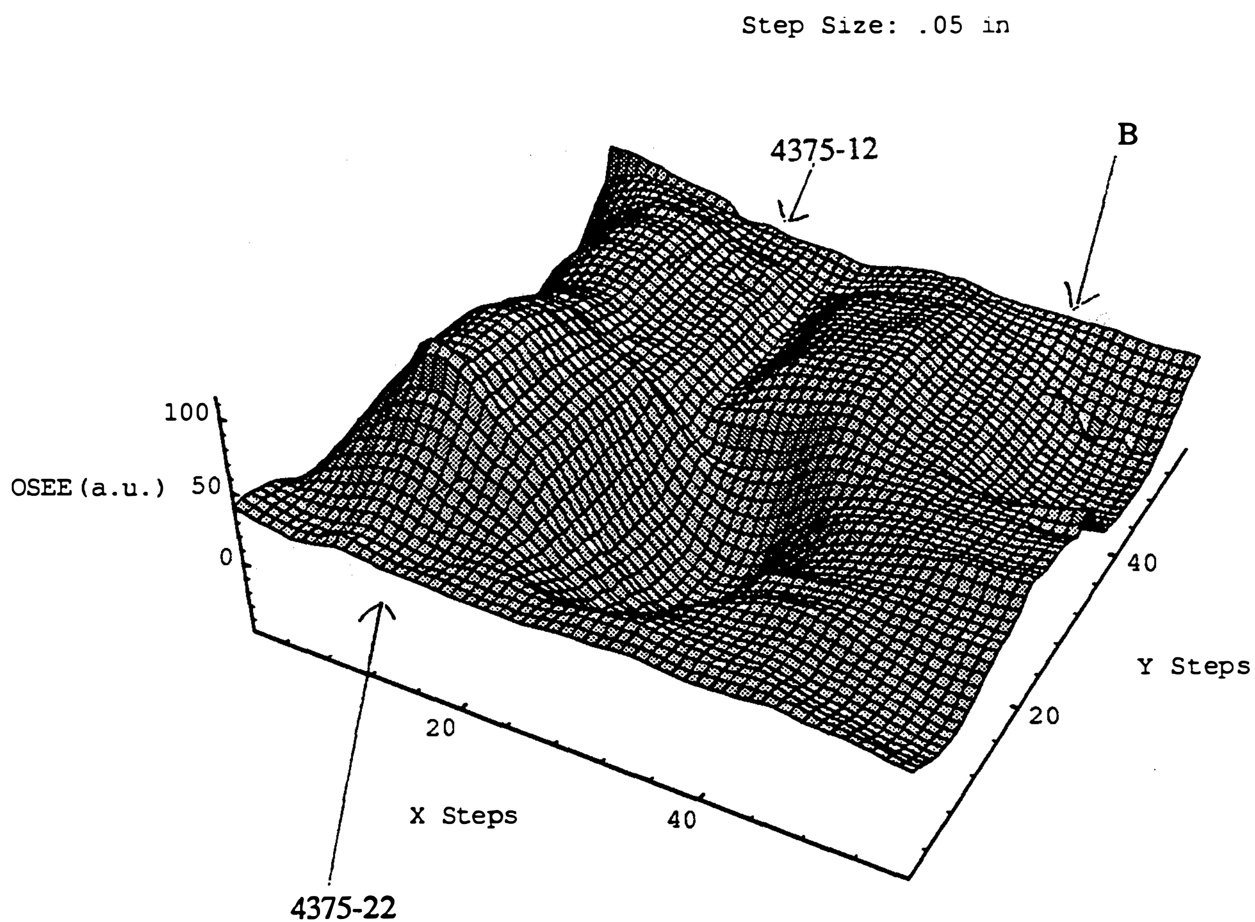


**Figure 30. Comparison of the photoemission in air between samples:**
**4375-12: textured ZnO from Solarex,**
**4375-22: textured ZnO from Harvard (Prof. Gordon's Group), and**
**B: virgin sample of 4375-21.**

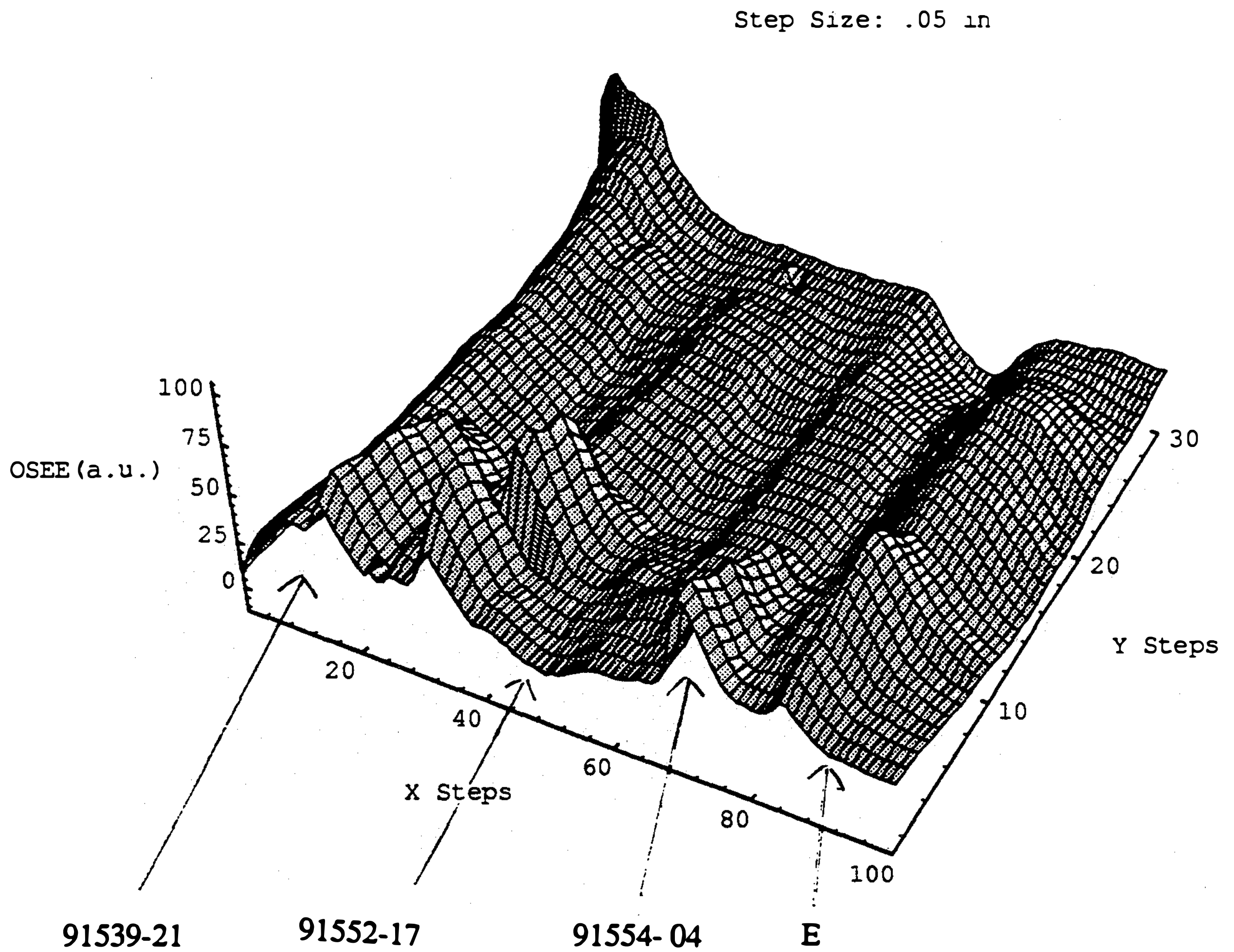


**Figure 31. Comparison of the photoemission in air between samples of: 91539-21: 1000 Å, specular Zn0 (no texture) sputtered at IEC, 91552-17: 200 Å, specular ZnO sputtered on textured $SnO_2$, 91554-04: 1000 Å, specular ZnO sputtered on textured $SnO_2$ and E: 1000 Å, specular $SnO_2$ grown on textured ZnO (Harvard).**

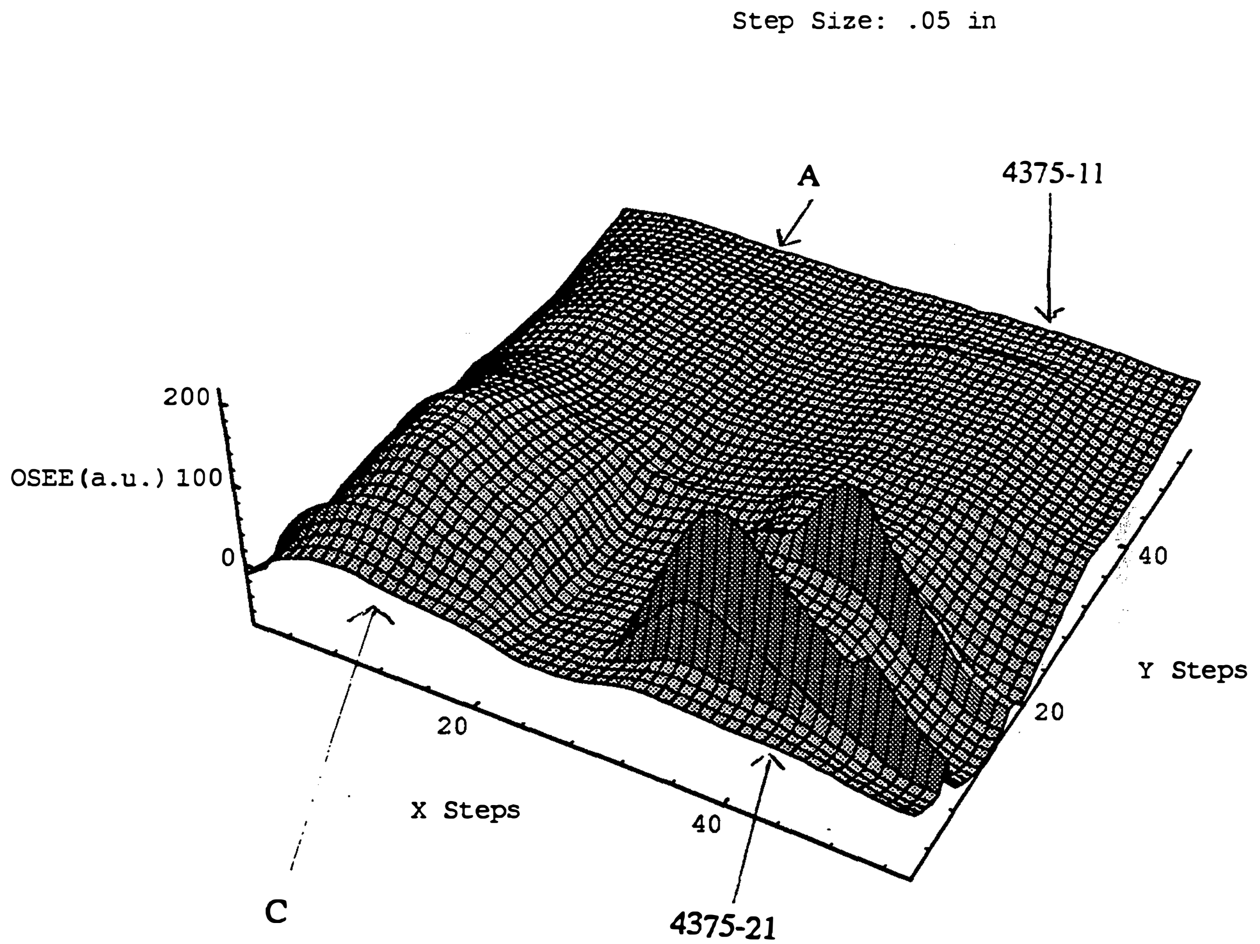


**Figure 32. Comparison of the photoemission in air between samples:**
**A: virgin sample of 4375-11,**
**C: virgin sample of 4375-21,**
**4375-11: textured $SnO_2$ from Solarex (standard device sample), and**
**4375-21: textured ZnO from Utility PV group (UPG).**

## Abstract

The technique of photoconductive frequency mixing was employed to separately determine the mobility and lifetime in a-Si:H and a-SiC:H. Light degradation studies reveal in addition to the decay of the photoconductivity and electron lifetime, continuous decay of the electron drift mobility was found during the light soaking process. The drift mobility ($\mu_d$) of intrinsic hydrogenated amorphous silicon (a-Si:H) films produced by both glow discharge and hot wire techniques increases with increasing electric field, while the lifetime ($\tau$) decreases with increasing electric field, and the $\mu\tau$ product is essentially independent of the electric field. We have also found that a greater field dependence of the drift mobility of an a-Si:H film in the annealed state indicates a poorer stability of the photoconductivity upon light soaking. This empirical relationship is consistent with earlier observation that light soaking decreases of the drift mobility in most a-Si:H based materials. This empirical relationship suggests that the Staebler-Wronski degradation of a-Si:H can be linked to defects that are responsible for the field dependence of the drift mobility in the annealed state. In addition, the effects of deposition temperature and hydrogen dilution ratio an the transport properties of a-Si:2H and a-SiC:H were investigated.

Photoemission measurements in air of a-Si:H, a-SiC:H and transparent conducting oxide layers revealed inhomogeneities of composition or surface contaminates.

# References


1. E. R. Giessinger, R. Braunstein, S. Dong, and B. G. Martin, *J. Appl. Phys.* **69**, 1469 (1991).

2. Yi Tang, R. Braunstein, and B. von Roedern, *Mat. Res. Soc. Symp. Proc.* **258**, 735 (1992).

3. Yi Tang, R. Braunstein, B. von Roedern, and F. R. Shapiro, *Mat. Res. Soc. Symp. Proc.* **297**, 407 (1993).

4. R. Braunstein and Yi Tang, *Proceedings of the 21st International Conference on Physics of Semiconductors* (August 1992), Beijing, China, 1, 269.

5. Yi Tang, R. Braunstein, and B. von Roedern, *Appl. Phys. Lett.* **63** (17), 2393 (1993).

6. R. Brüggemann, C. Main, J. Berkin, and S. Reynolds, *Phil. Mag. B* **62**, 29 (1990).

7. H. Oheda, *J. Appl. Phys.* **52**, **6693** (1981).

8. M. Stutzmann, W. B. Jackson, and C. C. Tsai, *Phys. Rev. B* **32**, 23 (1985).

9. T. J. McMahon and J. P. Xi, *Phys. Rev.B* **34**, 2475 (1986).

10. D. Redfield and R. H. Bube, *Phys. Rev. Lett.* **65**, 464 (1990).

11. R. Biswas, I. Kwon, and C. M. Soukoulis, *Phys. Rev. B* **44**, 3403 (1991).

12. M. Stutzmann, *Phil. Mag. B* **56**, 63 (1987).

13. M. Stutzmann, *Phil. Mag. B* **60**, 531 (1989).

14. J. Kakalios, R. A. Street, and W. B. Jackson, *Phys. Rev. Lett.* **59**, 1037 (1987).

15. W. B. Jackson, *Phys. Rev. B* **41**, 10257 (1990).

16. D. Adler, *Solar Cells* **9**, 133 (1982).

17. R. H. Bube, L. Benatar, and D. Redfield, *J. Appl. Phys.* **75**, 1571 (1994).

18. H. Fritzsche, *J. Non-Cryst. Solids* **6**, 49 (1971).

19. H. Overhof and W. Beyer, *Phil. Mag. B* **43**, 433 (1981).

20. H. M. Branz and M. Silver, *Phys. Rev. B* **42**, 7420 (1990).

21. B. von Roedern and A. Madan, *Phil. Mag. B* **63**, 293 (1991).

22. H. Overhof, *Mat. Res. Soc. Symp. Proc.* **258**, 681 (1992).

23. R. A. Street, *Appl. Phys. Lett.* **42**, 507 (1983).

24. N. Wyrsh and A. Shah, *Solid State Comm.*, **80**, 807 (1991).

25. Q. Wang, H. Antoniadis, and E. A. Schiff, *Appl. Phys. Lett.* **60**, 2791 (1992).

26. P. G. LeComber, A. Madan, and W. E. Spear, *J. Non-Cryst. Solids* **11**, 219 (1972).

27. R. H. Klazes, M. H. L. M. Van Den Broek, J. Bezemer, and S. Radelaar, *Phil. Mag.* **45**, 377 (1982).

28. M. H. Brodsky, M. A. Frisch, J. F. Ziegler, and W. A. Lanford, *Appl. Phys. Lett.* **30**, 561 (1977).

29. R. W. Collins, in *Amorphous Silicon and Related Materials*, edited by H. Fritzsche (World Scientific, Singapore, 1988), P. 1003.

30. C. R. Wronski, R. M. Dawson, M. Gunes, Y. M. Li, and R. W. Collins, *Mat. Res. Soc. Symp. Proc.* **297**, 443 (1993).

31. R. M. A. Dawson, C. M. Fortmann, M. Gunes, Y. M. Li, S. S. Nag, R. W. Collins, and C. R. Wronski, *Appl. Phys. Lett.* **63**, 955 (1993).

32. Y. -M. Li, A. Catalano, and B. F. Fieselmann, *Mat. Res. Soc. Symp. Proc.* **258**, 923 (1992).

33. Y. Lu, I. An, M. Gunes, M. Wakagi, C. R. Wronski, and R. W. Collins, *Mat. Res. Soc. Symp. Proc.* **297**, 31 (1993).Yi Tang, R. Braunstein, *Appl. Phys. Lett.* **66** (6), 721 (1995).

34. M. Silver and R. C. Jarnagin, *Mol. Cryst.* **3**, 461 (1968).

35. H. Fritzsche, *J. Non-Cryst. Solids* **6**, 49 (1971).

36. H. Overhof and W. Beyer, *Phil. Mag. B* **43**, 433 (1981).

37. D. Han and H. Fritzsche, J. Non-Cryst. Solids **59-60**, 398 (1983).

38. H. M. Branz and M. Silver, *Phys. Rev. B* **42**, 7420 (1990).

39. B. von Roedern and A. Madan, *Phil. Mag. B* **63**, 293 (1991).

40. H. Overhof and P. Thomas, "Electronic Transport in Hydrogenated Amorphous Semiconductors" (Berlin, Springer-Verlag), **114**, 108 (1989).

41. S. D. Baranovskii and M. Silver, *Phil. Mag. Lett.* **61**, 77 (1990).

42. J. A. Howard and R. A. Street, *Phys. Rev. B* **44**, 7935 (1991).

43. C. Witt, U. Haken, M. Hundhausen, and L. Ley, *Verhandlungen DPG (VI)*, **30**, HL 26.2, Physik Verlag (1995).

44. The statistical model is based on the idea that the drift mobility is proportional to the probability of a carrier going over the potential barrier through thermal activation. The role of the external field is to change the density of states inside the potential well, thus to change the probability and the mobility. The density of states is assumed to be proportional to the spacial range inside the potential well.

45. B. von Roedern, *Am. Inst. Phys. Conf. Proc.* **234**, 122 (1991).

46. Yi Tang and R. Braunstein, unpublished.

47. R. G. Palmer, D. l. Stein, E. Abrahams, and P. W. Anderson, *Phys. Rev. Lett.* **53**, 958 (1984).

# REPORT DOCUMENTATION PAGE

*Form Approved*
*OMB NO. 0704-0188*

Public reporting burden for this collection of information is estimated to average 1 hour per response, including the time for reviewing instructions, searching existing data sources, gathering and maintaining the data needed, and completing and reviewing the collection of information. Send comments regarding this burden estimate or any other aspect of this collection of information, including suggestions for reducing this burden, to Washington Headquarters Services, Directorate for Information Operations and Reports, 1215 Jefferson Davis Highway, Suite 1204, Arlington, VA 22202-4302, and to the Office of Management and Budget, Paperwork Reduction Project (0704-0188), Washington, DC 20503.

| 1. AGENCY USE ONLY (Leave blank) | 2. REPORT DATE | 3. REPORT TYPE AND DATES COVERED |
|---|---|---|
| | October 1995 | Annual Subcontract Report, 13 May 1994 - 12 May 1995 |

4. TITLE AND SUBTITLE

Photocharge Transport and Recombination Measurements in Amorphous Silicon Films and Solar Cells by Photoconductive Frequency Mixing

5. FUNDING NUMBERS

C: XAN-4-13318-10

TA: PV531101

6. AUTHOR(S)

R. Braunstein, Y. Tang, S. Dong

7. PERFORMING ORGANIZATION NAME(S) AND ADDRESS(ES)

University of California
Los Angeles, California

8. PERFORMING ORGANIZATION REPORT NUMBER

9. SPONSORING/MONITORING AGENCY NAME(S) AND ADDRESS(ES)

National Renewable Energy Laboratory
1617 Cole Blvd.
Golden, CO 80401-3393

10. SPONSORING/MONITORING AGENCY REPORT NUMBER

TP-451-20019

DE95013131

11. SUPPLEMENTARY NOTES

NREL Technical Monitor: B. von Roedern

12a. DISTRIBUTION/AVAILABILITY STATEMENT

12b. DISTRIBUTION CODE

UC-1262

13. ABSTRACT *(Maximum 200 words)*

This report describes work performed by the University of California at Los Angeles (UCLA) during Phase I of a subcontract with members of the National Renewable Energy Laboratory (NREL) Wide-Band-Gap Alloy Team and the Metastability and Mid-Band-Gap Alloy Team. Work was conducted in a number of areas. The technique of photoconductive frequency mixing was employed to separately determine the mobility and lifetime in a-Si:H and a-SiC:H. The effects of deposition temperature and hydrogen dilution ratio and the transport properties of a-Si:H and a-SiC:H were investigated. Measurements of the electric field dependence of the drift mobility indicated that an empirical relationship exists between the field dependence and the stability of a-Si:H. In-air scanning photoemission measurements of bare and a-Si:H-coated transparent conductor surfaces revealed inhomogeneities of composition or surface contaminates.

14. SUBJECT TERMS

photocharge ; transport ; recombination ; measurements ; amorphous silicon films ; photoconductivity ; photovoltaics ; solar cells

15. NUMBER OF PAGES
72

16. PRICE CODE

| 17. SECURITY CLASSIFICATION OF REPORT | 18. SECURITY CLASSIFICATION OF THIS PAGE | 19. SECURITY CLASSIFICATION OF ABSTRACT | 20. LIMITATION OF ABSTRACT |
|---|---|---|---|
| Unclassified | Unclassified | Unclassified | UL |

NSN 7540-01-280-5500

Standard Form 298 (Rev. 2-89
Prescribed by ANSI Std. Z39-1
298-1(